Katharina Huber, BSc

The metabolic flux of fatty acids in *Saccharomyces cerevisiae*

MASTERARBEIT

zur Erlangung des akademischen Grades

Master of Science

Masterstudium Biochemie und Molekulare Biomedizin

eingereicht an der

Technischen Universität Graz

Betreuer

Univ.-Prof. DI Dr.techn. Sepp-Dieter Kohlwein

Dr. Harald F. Hofbauer

Institut für Molekulare Biowissenschaften

Universität Graz

Graz, Mai 2014

Katharina Huber, BSc

The metabolic flux of fatty acids in *Saccharomyces cerevisiae*

MASTER THESIS

for attainment of the degree

Master of Science

submitted to

Graz University of Technology

Supervision

Univ.-Prof. DI Dr.techn. Sepp-Dieter Kohlwein

Dr. Harald F. Hofbauer

Institute of Molecular Biosciences

University of Graz

Graz, May 2014

EIDESSTATTLICHE ERKLÄRUNG
AFFIDAVIT

Ich erkäre an Eides statt, dass ich die vorliegende Arbeit selbstständig verfasst, andere als die angegebenen Quellen/Hilfsmittel nicht benutzt, und die den benutzten Quellen wörtlich und inhaltlich entnommenen Stellen als solche kenntlich gemacht habe. Das in TUGRAZonline hochgeladene Textdokument ist mit der vorliegenden Masterarbeit identisch.

I declare that I have authored this thesis independently, that I have not used other than the declared sources/resources, and that I have explicitly indicated all material which has been quoted either literally or by content from the sources used. The text document uploaded to TUGRAZonline is identical to the present master's thesis.

_____ _____

Datum / Date Unterschrift / Signature

Acknowledgments

I would like to express my gratitude to Univ.-Prof. DI Dr. Sepp-Dieter Kohlwein, for the opportunity to do my master thesis under his supervision as well as for his excellent guidance and support during this time.

I would also like to thank Dr. Harald F. Hofbauer, Dr. Gerald "Niki" Rechberger and all my colleagues for their ongoing help in all scientific questions. Your advice and introduction to various scientific techniques were invaluable to me. Thank you also for making the lab a friendly working environment and the wonderful time we spent together outside of work.

Special thanks go to my family, my boyfriend Manuel and all my friends. I have no words to express my deepest appreciation for always believing in me, and your constant support throughout the entire process.

A big thank you to you all!

Abstract

Defects in fat homeostasis are caused by an imbalanced synthesis and degradation of lipids and contribute substantially to the pathogenesis of lipid-related disorders like obesity, insulin resistance, type-2 diabetes mellitus, cardiovascular disease as well as cancer. Over the past years, lipidomic studies provided insights into the dynamics of lipid metabolism by stable isotope labeling techniques in combination with mass spectrometry. However, most of these techniques are very expensive or do not permit investigation of endogenous fatty acid *de novo* biosynthesis and their incorporation into glycerolipids. Here, we report a novel technique for monitoring phospholipid and neutral lipid synthesis, which employs a specific “mass-tag” strategy by pre-cultivation of cells in ^{13}C glucose to steady state. By shifting cells back to media containing ^{12}C glucose, the recovery rates of unlabeled lipid species are determined by mass spectrometry. Analysis of wild type and selected mutant strains enabled the determination of *de novo* synthesis routes and remodeling dynamics of lipid species. As a proof of concept, this method was applied to study the contribution of the glycerol-3-phosphate acyltransferase Gpt2 and the Kennedy pathway to phospholipid and neutral lipid synthesis and turnover. The results indicate a specific role of the acyltransferase in phospholipid synthesis during logarithmic growth, whereas inhibition of the Kennedy pathway did not affect phospholipid-labeling kinetics. In conclusion, the described method enables dynamic lipidomic studies of phospho- and neutral lipid metabolism to reveal the specific contributions of acyltransferases to the metabolic flux of fatty acids into phospholipids and neutral lipids *in vivo*.

Zusammenfassung

Eine Störung der zellulären Lipidhomöostase durch unausgeglichenen Auf- oder Abbau von Lipiden trägt wesentlich zur Pathogenese von lipidbedingten Erkrankungen wie Adipositas, Typ-II Diabetes mellitus, Herz-Kreislauferkrankungen sowie Krebs bei. In den letzten Jahren hat die Anwendung von Isotopenmarkierungstechniken in Kombination mit der Massenspektrometrie (MS) Einblicke in die Dynamik des Lipidstoffwechsels gegeben. Die meisten Techniken sind allerdings sehr teuer oder liefern keine ausreichenden Informationen über die endogene Fettsäurebiosynthese und den Einbau von Fettsäuren in Lipide. Wir haben eine neuartige Methode zur Detektion von Phospho- und Neutrallipiden entwickelt. Das Verfahren verwendet eine spezielle "Mass-Tag"-Strategie, wobei durch Vorkultivierung von Zellen in ^{13}C-markierter Glukose Lipidspezies mit entsprechender Kohlenstoff-spezifischer Massenzunahme produziert werden. Durch das Rücküberführen der Zellen in Medium mit ^{12}C Glukose, können neu synthetisierte Lipidmoleküle mittels MS bestimmt werden. Die Analyse des Wildtyps und verschiedener Mutantenstämme zeigte eine schnelle Kinetik, welche die Bestimmung der *de novo* Syntheserate und Remodeling-Dynamiken einzelner Lipidspezies ermöglichte. Die Methode wurde angewandt, um den Einfluss der Glycerin-3-phosphat Acyltransferase Gpt2 und des Kennedy-Syntheseweges auf die Phospho- und Neutrallipid Synthese zu untersuchen. Die Ergebnisse deuten auf eine spezifische Rolle der Acyltransferase im Phospholipid Metabolismus hin, wobei die Hemmung des Kennedy Syntheseweges die Acylierungs-Kinetik nicht beeinflusste. Das beschriebene Verfahren ermöglicht dynamische Lipidstudien des Phospho- und Neutrallipidstoffwechsels, um den spezifischen Beitrag der Acyltransferasen zum Fluss von Fettsäuren ins Phospholipid und Neutrallipid *in vivo* zu entschlüsseln.

Table of contents

Abbreviations

Abbreviation	Name
Acetyl-CoA	acetyl-coenzyme A
ACL	ATP-citrate lyase
CDP	cytidine diphosphate
DAG	diacylglycerol
FA	fatty acid
FAD	flavin adenine dinucleotide
FAS	fatty acid synthase
GPI	glycerophosphoinositol
HAT	histone acetyltransferase
LCFA	long chain fatty acid
NAD	nicotinamide adenine dinucleotide
NPLC	normal phase liquid chromatography
Opi^{-}	overproducer of inositol
PA	phosphatidic acid
PC	phosphatidylcholine
PDC	pyruvate dehydrogenase complex
PDME	phosphatidyldimethylethanolamine
PE	phosphatidylethanolamine
PI	phosphatidylinositol
PL	phospholipid
PMME	phosphatidylmonomethylethanolamine
PS	phosphatidylserine
RFLC	reversed phase liquid chromatography
TAG	triacylglycerol
TPP	thiamine pyrophosphat
UAS	upstream activating sequence

1 Introduction

Cellular lipid and energy homeostasis is a crucial process for every organism to ensure metabolic equilibrium conditions. To achieve lipid homeostasis adapted to nutritional and environmental conditions, a complex network of genes, feedback mechanisms and points of regulation are required. Furthermore, to enable proper cellular growth and cell division, a balanced uptake and utilization of energy substrates is important and “over-nutrition condition” has to be compensated.

The lapse of cellular fat homeostasis results in imbalanced fatty acids and lipid species composition and subsequently in cell dysfunction or even cell death. These alterations in the lipid buildup contribute substantially to the pathogenesis of lipid-associated disorders such as obesity, insulin resistance, type-2 diabetes mellitus, cardiovascular disease, cancer and neurodegenerative diseases. The rapid spread and increase of lipid-associated disorders has become a world wide problem and moved lipid metabolism into the focus of biomedical research (Kohlwein, 2010a; Vihervaara et al., 2013). A suitable model for studying lipotoxic scenarios is the yeast *Saccharomyces cerevisiae*, owing the convenience concerning genetic manipulation, growth conditions, short generation time and availability of the whole yeast genome sequence (Goffeau et al., 1996; Natter and Kohlwein, 2012). The enzymes in metabolic pathways and regulatory networks are functionally conserved across the eukaryotic kingdom from yeast to human (Henry et al., 2012; Kurat et al., 2006). Therefore, yeast studies play an important role to understand triacylglycerol homeostasis (Kohlwein, 2010), lipid-induced cell dysfunction and cell death (Kohlwein, 2010a; Kohlwein and Petschnigg, 2007). Over the past several years, lipidomic studies generated insights into lipid-related processes by investigating the specific roles of lipid species in disorders. Lipidomics approaches have been applied to identify potential targets for the treatment of lifestyle-related diseases as well as genetic conditions (Hu et al., 2009; Murphy and Nicolaou, 2013; Vihervaara et al., 2013).

1.1 Lipid synthesis in the yeast *Saccharomyces cerevisiae*

1.1.1 Fatty acids in yeast

Fatty acids are essential components of biological membranes, play an important role in signaling pathways and are a suitable form to store metabolic energy. In yeast, the fatty acid repertoire is rather simple compared to the mammalian system. The predominant long chain fatty acids (LCFA) are palmitic acid (C16:0), palmitoleic acid (C16:1), stearic acid (C18:0) and oleic acid (C18:1) and to a minor extent lauric acid (12:0), myristic acid (C14:0), myristoleic acid (C14:1), and saturated very long chain fatty acids (VLCFA) consisting of 20-26 carbon atoms (Klug and Daum, 2014; De Kroon et al., 2013). VLCFA occur mainly in glycerophosphoinositol (GPI) anchors and sphingolipids (Cowart and Obeid, 2007; Fujita and Jigami, 2008). Fatty acids differ form each other not only in chain length but also in the degree of saturation. The saturation level is under control of the *delta-9* fatty acid desaturase Ole1, which introduces a *cis*-double bond between the C9 and C10 carbon atoms of acyl-CoA molecules (Stukey et al., 1990). Cellular fatty acids derive mainly from *de novo* synthesis. However, exogenous fatty acids and fatty acids from endogenous lipid turnover can be efficiently incorporated into lipid species (Tehlivets et al., 2007). Fatty acid transport proteins required for exogenous uptake are Fat1, Faa1 and Faa4 (Faergeman et al., 1997, 2001). The reactivation of free fatty acids, derived from membrane lipid degradation, is executed by Faa1, Faa2 and Faa3, whereas Faa4 participates in the activation of fatty acids derived from triacylglycerol and steryl ester breakdown (Black and DiRusso, 2007).

1.1.2 Acetyl-coenzyme A

Acetyl-coenzyme A (acetyl-CoA) is a precursor for various biosynthetic pathways. In *S. cerevisiae,* the biosynthesis of acetyl-CoA is mainly achieved by glycolysis-produced pyruvate, when cells are grown on fermentable sugars such as glucose. In the first step, pyruvate decarboxylase (Pdc1, Pdc5 and Pdc6) executes the decarboxylation of pyruvate to acetaldehyde and carbon dioxide. The subsequent conversion of acetaldehyde to acetate is catalyzed by acetaldehyde dehydrogenase (Ald2, Ald3, Ald4, Ald5, Ald6) (Pronk et al., 1996). Afterwards, acetate is converted to acetyl-CoA catalyzed by acetyl-CoA synthetase, which is encoded by two structural

genes in yeast, *ACS1* and *ACS2* (van den Berg et al., 1996). Cytosolic acetyl-CoA is the only source for fatty acid biosynthesis, by serving as substrate for the acetyl-CoA carboxylase and subsequently for the fatty acid synthase (FAS) complex (Chen et al., 2012). Furthermore, nucleocytosolic acetyl-CoA is used for chromatin regulation as it serves as substrate for histone acetylation by histone acetyltransferases (HATs) (Takahashi et al., 2006). In mammalian cells, the majority of acetyl-CoA for histone acetylation is generated by ATP-citrate lyase (ACL) (Wellen et al., 2009). However, *S. cerevisiae* lacks ACL, which is responsible for translocation of acetyl-CoA across the mitochondrial membrane (Boulton and Ratledge, 1981). Therefore, fatty acid *de novo* synthesis and histone acetylation compete for the same acetyl-CoA pool (Galdieri and Vancura, 2012). During glucose-limited respiratory growth, pyruvate is metabolized to acetyl-CoA via the mitochondrial pyruvate dehydrogenase complex (PDC) (Pronk et al., 1996). PDC is a multi-enzyme complex, which consists of the three enzymes pyruvate dehydrogenase, dihydrolipoyl transacetylase and dihydrolipoyl dehydrogenase and requires the 5 coenzymes or prosthetic groups called thiamine pyrophosphate (TPP), flavin adenine dinucleotide (FAD), coenzyme A, nicotinamide adenine dinucleotide (NAD) and lipoate. Acetyl-CoA achieved through the PDH serves as fuel for the tricarboxylic acid (TCA) cycle to produce energy in form of ATP (Chen et al., 2012). In the absence of glucose, fatty acids are catabolized to acetyl-CoA by peroxisomal ß-oxidation in a 4 step reaction with the help of the enzymes acyl-CoA oxidase, enoyl-CoA hydratase, 3-hydroxyacyl-CoA dehydrogenase, and 3-ketoacyl-CoA thiolase. Finally, the product of fatty acid oxidation, acetyl-CoA, is further oxidized to CO_2 in the citric acid cycle in the mitochondria. Therefore, acetyl-CoA is exported via the carnitine-dependent acetyl-CoA transport or via the glyoxylate cycle (Kohlwein et al., 2013). Additionally, the carbon skeleton of amino acids can be oxidized to intermediates of the citric acid cycle such as acetyl-CoA, α-ketoglutarate, succinyl-CoA, fumarate and oxaloacetate. Some amino acids are catabolized to pyruvate, which can be further used to yield acetyl-CoA. Besides its function as an important metabolic intermediate in fatty acid biosynthesis and energy metabolism, acetyl-CoA is also an important building block for the biosynthesis of waxes, flavonoids, certain amino acids, carotenoids, polyhydroxyalkanoates, polyketides, butanol and isoprenoids (Chen et al., 2012).

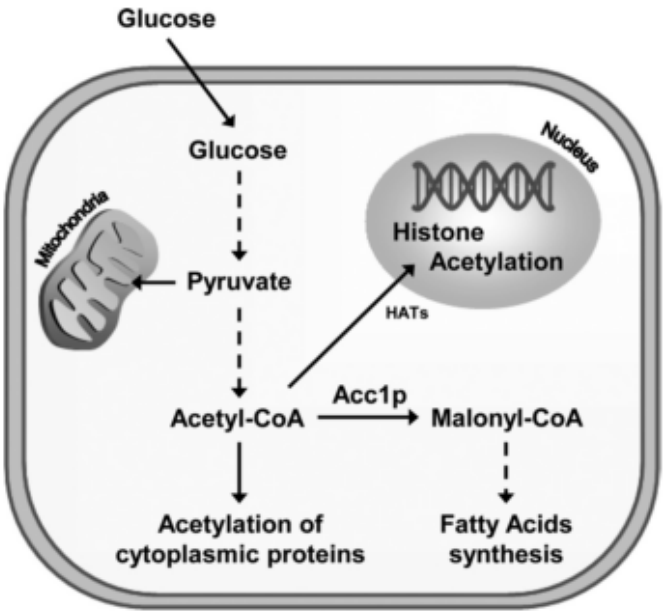

Figure 1: Schematic representation of acetyl-CoA metabolism, adapted from Galdieri and Vancura, 2012.

1.1.2.1 Fatty acid *de novo* synthesis

Fatty acid *de novo* synthesis starts with the carboxylation of acetyl-CoA to malonyl-CoA by the rate limiting enzyme acetyl-CoA carboxylase (Acc1) (Hasslacher et al., 1993). Malonyl-CoA molecules serve as C_2-donors in further multistep condensation reactions. The cytosolic fatty acid synthase complex (FAS complex), composed of α- and β-subunits encoded by *FAS2* and *FAS1*, extend acetyl-CoA by adding malonyl-CoA as C_2-donor in each elongation cycle to yield up to 16C and 18C acyl-CoAs. The 3-ketoacyl-CoA synthase, Elo1, acts together with the FAS complex and is responsible for the production of C14, C16 and C18 acyl-CoAs, whereas the condensing enzyme Elo2 is responsible for the synthesis of FAs up to C22 carbon atoms and Elo3 up to C26 carbon atoms (Oh et al., 1997; Tehlivets et al., 2007).

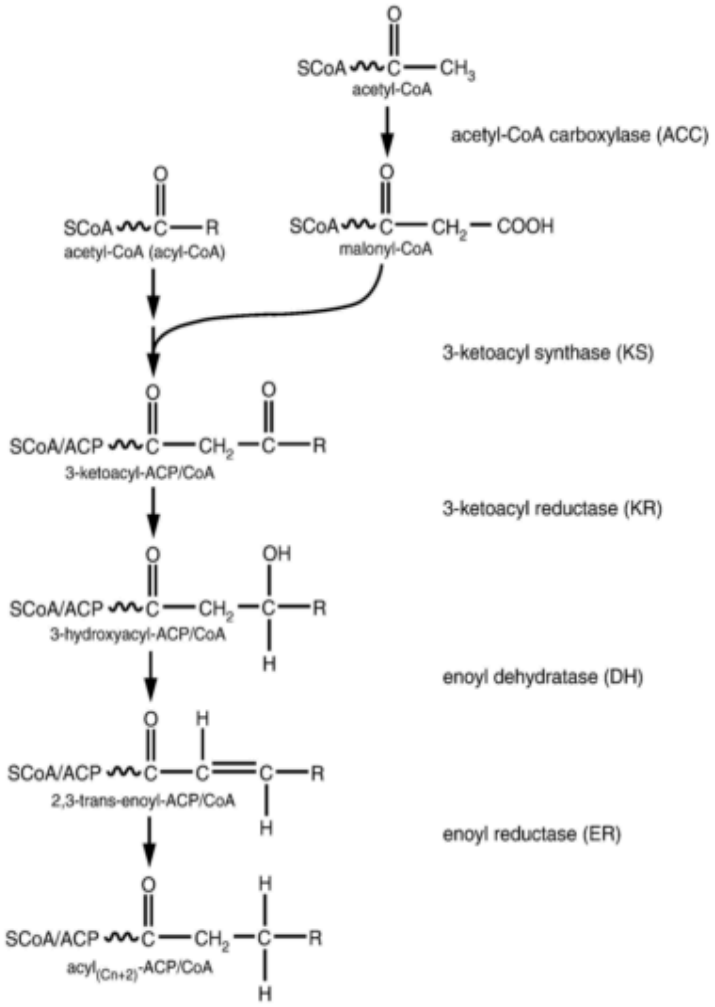

Figure 2: Fatty acid synthesis and elongation in *Saccharomyces cerevisiae,* adapted from Tehlivets et al., 2007.

1.1.3 Phospholipid biosynthesis

Phospholipids are built up from hydrophobic acyl-chains esterified to a glycerol-3-phosphate backbone. The saturated fatty acids predominate at the *sn-1* position, whereas unsaturated fatty acids are mainly esterified to the *sn-2* position (Wagner and Paltauf, 1994). Phospholipids are classified, according to the nature of their head group in phosphatidylcholine (PC), phosphatidylethanolamine (PE) phosphatidylserine (PS), phosphatidylinositol (PI) and phosphatidic acid (PA). Each class consists of a plethora of molecular species determined by the length and saturation level of the acyl chain. Phospholipids are the main building blocks for biological membranes, which represent a 5-9 nm barrier to the environment or sub-divide cells into intracellular compartments (De Kroon et al., 2013). The lipid composition in membranes is highly defined but capable for variations to adapt to environmental conditions such as temperature, culture medium, carbon source and growth phase, to maintain lipid homeostasis (Chatterjee et al., 2001; Tuller et al.,

1999; Wagner and Paltauf, 1994). In the phospholipid biosynthetic pathway, numerous enzymes are involved, which show homology between yeast and higher eukaryotes. The phospholipid synthesis starts with the esterification of an acyl-CoA to the *sn*-1 position of glycerol-3-phosphate initiated by Gpt2/Gat1 or Sct1/Gat2 to yield lyso-PA (Zheng and Zou, 2001). Gpt2 and Sct1 also utilize a second metabolite from the glycolysis pathway, dihydroxyacetone phosphate, to generate 1-acyl-DHAP, which is converted to lyso-PA by Ayr1 (Athenstaedt and Daum, 2000). Afterwards, a second acyl-chain is transferred to the *sn*-2 position of a lyso-PA to generate PA by Slc1 or Ale1 (Benghezal et al., 2007). PA is further processed to diacylglycerol (DAG) by Pah1 (Han et al., 2006) or metabolized to CDP-DAG by Cds1 (Shen et al., 1996), the common precursors for neutral lipid and phospholipid biosynthesis, respectively. A detailed description of neutral lipid synthesis and degradation is reviewed in the literature (Henry et al., 2012; Kohlwein et al., 2013). CDP-DAG is utilized to synthesize PI by the *PIS1*-encoded PI synthase (Nikawa and Yamashita, 1984; Paulus et al., 1960). The inositol used in this reaction can be produced *de novo* out of glucose-6-phosphate by inositol-3-phosphatesynthase Ino1 (Klig and Henry, 1984) and by inositol-3-phosphatephosphatase Inm1 (Murray and Greenberg, 2000). Exogenously supplied inositol can be taken up efficiently by inositol permeases Itr1 and Itr2 (Nikawa et al., 1991). The enzyme PS synthase Cho1 also uses CDP-DAG as substrate for the synthesis of PS (Letts et al., 1983). Furthermore, CDP-DAG is the precursor for phosphatidylglycerol (PG) and cardiolipin (CL), a major lipid in mitochondrial membranes (Schlame et al., 2000). In yeast, two different pathways exist for the formation of PE and PC: the CDP-DAG and the CDP-choline or Kennedy pathway (De Kroon et al., 2013).

1.1.3.1 CDP-DAG pathway

PS is the precursor in the CDP-DAG pathway for the synthesis of PE and PC. In the first step, PS is decarboxylated to PE by the PS decarboxylases Psd1 (Clancey et al., 1993; Trotter et al., 1993) and Psd2 (Trotter et al., 1995).

In the following three methylation steps, Cho2/Pem1 (Kodaki and Yamashita, 1987; Summers et al., 1988) transfers a methyl group to PE to form phosphatidylmonomethylethanolamine (PMME) which is further methylated by Opi3/Pem2 yielding phosphatidyldimethylethanolamine (PDME) and PC (McGraw and Henry, 1989). The methyl donor for this catalytic reaction is S-adenosyl-L-methionine (Tehlivets et al., 2004).

1.1.3.2 Kennedy pathway

The second biosynthetic route to produce PE and PC is the CDP-choline pathway, better known as the Kennedy pathway (Kennedy and Weiss, 1956). Therefore, an activated CDP-ethanolamine or CDP-choline is transferred to DAG yielding PE or PC by Ept1 (Hjelmstad and Bell, 1988) and Cpt1, respectively (Hjelmstad and Bell, 1987). The activation occurs in a two step mechanism by phosphorylation of ethanolamine by the cytosolic ethanolamine kinase Eki1 to phosphoethanolamine and conversion to CDP-ethanolamine by ethanolamine-phosphate cytidylyltransferase Ect1 (Kim et al., 1999; Min-Seok et al., 1996). The PC synthesis is catalyzed in the same fashion by the enzymes choline kinase Cki1 (Hosaka et al., 1989) and cholinephosphate cytidylyltransferase Pct1, whereby Pct1p is the rate-limiting step of the CDP-choline pathway in the absence of choline (McMaster and Bell, 1994a; Tsukagoshi et al., 1987). The enzymes Ek1, Ept1, Cki1 and Cpt1 are not specific for PE or PC synthesis, because they show overlapping substrate specificity (Hjelmstad and Bell, 1991; Kim et al., 1999), whereas Ect1 and Pct1 show substrate specificity for PE and PC synthesis, respectively (Min-Seok et al., 1996; Tsukagoshi et al., 1987). The Kennedy pathway also functions as a recycling route for choline. PC, synthesized through the CDP-DAG pathway can be hydrolyzed to PA and choline by the yeast phospholipase D, Spo14. Choline, gained from this turnover is reassembled into PC by the Kennedy pathway (Carman and Han, 2011).

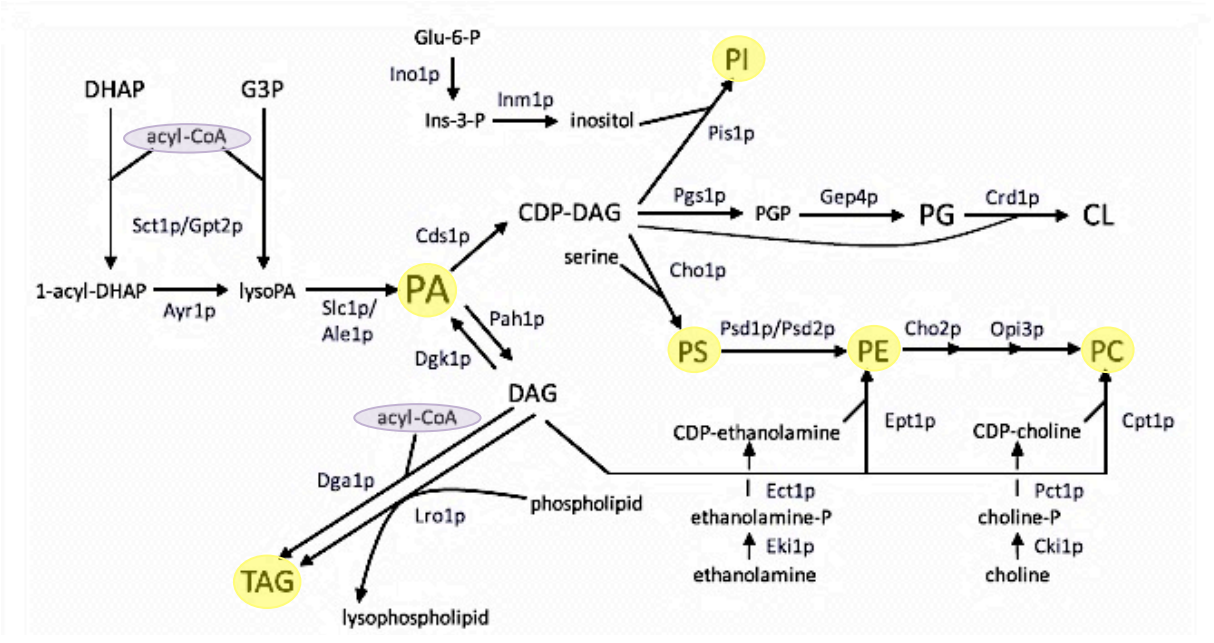

Figure 3: Lipid metabolism in *Saccharomyces cerevisiae,* adapted from De Kroon et al., 2013.

1.1.4 Phospholipid turnover

Phospholipid turnover can be achieved through phospholipase-mediated turnover or phospholipid remodeling by acyl-chain exchange. Phospholipases can be divided depending on the position they cleave off fatty acids or head groups from phospholipids. Phospholipase A_1 and A_2 cleave off fatty acids specifically on *sn-1* and *sn-2* position, respectively, whereas phospholipase B enzymes encoded by *NTE1*, *PLB1*, *PLB2* and *PLB3* hydrolyze fatty acids independent of their position (Merkel et al., 2005; Zaccheo et al., 2004).

Phospholipase C and D enzymes cleave off the head group of phospholipids, yielding DAG and PA, respectively (Flick and Thorner, 1993; Rudge et al., 2001).

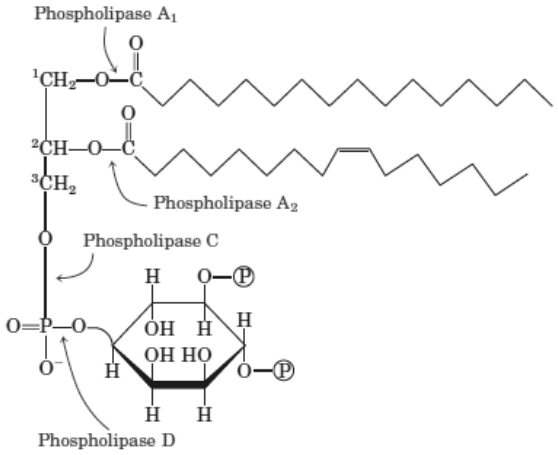

Figure 4: Scheme of a phospholipid and the site of action of phospholipases, adapted from Lehninger, 2008.

1.1.5 Acyl-chain remodeling

In the “Lands’ cycle”, acyl-chain remodeling is described as the post-synthetic modification of the phospholipid profile via deacylation by phospholipases to lyso-phosphate or glycerophosphodiester intermediates and acyl-CoA-dependent reacylation. Alternatively, remodeling takes place as an acyl-CoA independent transfer of an acyl-chain between glycerolipids by transacylases (Yamashita et al., 1997).

Enzymes involved in acyl-chain remodeling include the 1-acylglycerol-3-phospate-O-acyltransferase (AGPAT) family, O-acyltransferases (MBOAT) as well as lysophospholipid acyltransferases (LPLATs) (Shindou et al., 2009).

1.1.6 Regulation of phospholipid synthesis

To maintain lipid homeostasis within the cell, the lipid synthesis is regulated at the level of gene expression, posttranslational modification, intrinsic metabolites and enzyme activity.

1.1.6.1 UAS_{INO} regulation

Phosphatidic acid is the precursor for the biosynthesis of all glycerophospholipids. Its lipid content influences the transcription of genes possessing an inositol-responsive element (UAS_{INO}) (Henry et al., 2012). When PA levels are high, the repressor Opi1 and an auxiliary protein Scs2 can bind to PA located in the ER, whereby the translocation of Opi1 into the nucleus is prohibited. Therefore, the transcription factors Ino2 and Ino4 can bind to the UAS_{INO} element and enable gene expression. The depletion of PA induces the abolishment of the Opi1 / PA interaction and Opi1 translocates into the nucleus, where it builds a heterodimer with Ino2, and represses all UAS_{INO} genes (Carman and Henry, 2007; Henry et al., 2012; Loewen et al., 2004). Exogenously supplied inositol is assimilated through the transport proteins Itr1 and Itr2 (Nikawa et al., 1991) and leads to a decrease in PA levels by its drain into PI synthesis (Carman et al., 2009).

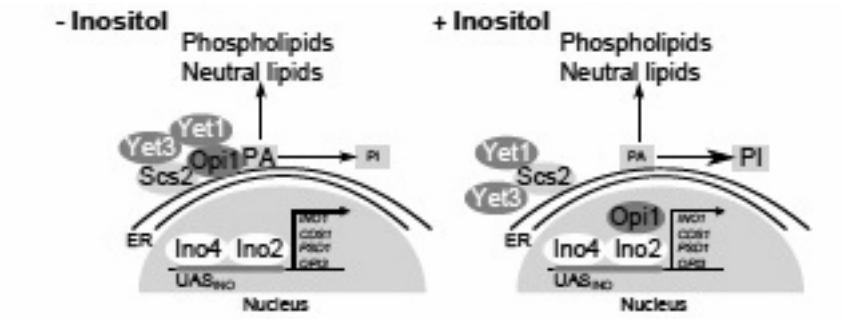

Figure 5: Regulation of the phospholipid biosynthetic genes by inositol (modified from (Carman and Han, 2011))

1.1.6.2 Regulation by zinc

The zinc-sensing transcription factor Zap1 also plays a crucial role in transcriptional regulation, by controlling the activation of genes containing the zinc-responsive *cis*-acting element UAS_{ZRE} (Han et al., 2005). Zinc depletion stimulates the expression of *PIS1* and *PAH1* and causes changes in phospholipid composition. The increased PI synthesis leads to PA consumption and thus, Opi1-mediated repression of UAS_{INO} containing genes. Besides induction of PI and depletion of PE, the levels of PC

remain unaffected (Yamashita et al., 1997), due to up-regulation of the Kennedy pathway enzymes Cki1 (Soto and Carman, 2008) and Eki1 (Kersting and Carman, 2006).

1.1.6.3 CTP / CDP-DAG mediated regulation

CTP is the precursor of intermediates of the CDP-DAG and Kennedy pathway, because it can be converted to CDP-DAG, CDP-choline and CDP-ethanolamine (Chang and Carman, 2008). CTP synthetase is allosterically inhibited by the intracellular concentration of CTP. CTP also inhibits the PS synthase activity (McDonough et al., 1995) and promotes the Kennedy pathway for phospholipid biosynthesis. Moreover, phospholipid synthesis is controlled by CDP-DAG-mediated regulation, which causes up-regulation of Pah1 activity (Wu and Carman, 1996) and inhibition of Dgk1 activity (Han et al., 2008). This results in increased levels of DAG, which can be either channeled into phospholipids or the neutral lipid TAG (Carman and Han, 2011).

1.1.6.4 Regulation by phosphorylation

In addition, phosphorylation by the enzymes protein kinase A, protein kinase C, casein kinase II and the cyclin-dependent protein kinase plays a key role in the regulation of membrane lipid composition to maintain proper regulation, cell cycle progression and cellular growth in response to varying environmental conditions (Thevelein, 1994). Protein kinases can affect the catalytic activity, the localization, the interaction with DNA and proteins and stability of particular regulatory proteins. Phosphorylation targets are phospholipid enzymes including the PS synthase (Cho1), the CTP synthase (Ura7), the choline kinase (Cki1), the PA phosphatase (Pah1) and the repressor of UAS_{INO} – containing genes, Opi1 (Carman and Han, 2011).

Taken together, the lipid metabolism is tightly controlled on various levels in a complex network of biochemical pathways. To study the influence of the regulation on the lipid profile during cell growth, lipidomic techniques such as mass spectrometry are required to unravel the flux of fatty acids, lipid synthesis rates and remodeling dynamics.

2 Lipidomics

Lipidomic investigations focus not only on the characterization of the entire compliments of lipids but also on the comprehensive understanding of function and impact on biological systems, in terms of membrane composition, cell signaling and adaptation to the environmental conditions (Hu et al., 2009; Watson, 2006) . Lipids display a complex variety of hundreds to thousand of individual species, to afford all diverse functions within the cell (Ejsing et al., 2009; Guan et al., 2009; Hunte and Richers, 2008). Recent technological advances and the implementation of high-throughput methods enable a sensitive and rapid detection of lipid composition (Watson, 2006). In the last decade, lipid profiling deepens the knowledge of the specific roles of lipids in health and lipid-associated diseases by elucidating therapeutic targets for human health (Hu et al., 2009).

2.1 Analytical methods in lipidomics

In the early time of lipidomics, traditional chromatographic methods for lipid analysis were used to separate lipids into distinct classes by liquid chromatography e.g. thin layer chromatography (TLC), or to separate certain lipid classes into specific molecular species by high-performance liquid chromatography (HPLC) (Hu et al., 2009; Touchstone, 1995).

2.1.1 Thin layer chromatography

The basic principle of all forms of chromatography is the separation of a mixture of substances into the individual components. In TLC, the stationary phase is composed of an absorbent (silica gel or aluminum oxide) mounted on a carrier plate. The sample is applied on the bottom of the plate in form of a spot and the plate is placed into a glass chamber. The mobile phase is located at the bottom of this glass chamber, a distance under the sample spot and moves as a result of capillary forces to the top of the thin layer plate, whereby the individual components of the lipid mixture are separated according to their affinity to the stationary phase. A detailed description about absorbents, sample preparation, selection of solvents and visualization and identification of lipids is reviewed in the literature (Fuchs et al., 2011; Mangold, 1961). The easy handling of the method makes it still an applicable

technique. However, the sometimes poor reproducibility is a major disadvantage. In addition to the lack of sensitivity, which makes it difficult do investigate low abundant lipid classes, the low resolution limits its area of application. Moreover, large sample volumes and multiple-step processes for sample preparation are required. Therefore, TLC represents a fast, simple and inexpensive method for lipid analysis, but only separates lipid classes, without distinction of molecular lipid species composition (Li et al., 2011; Pulfer and Murphy, 2003).

2.1.2 High performance liquid chromatography

High performance liquid chromatography (HPLC) is a frequently used technique in lipidomics because of its advantages in high resolution and good reproducibility (Li et al., 2011). Two different modes of HPLC can be applied such as normal-phase (NP) LC and reversed-phase (RP) LC; RPLC is commonly used in lipidomics, because it separates lipids according to their hydrophobicity. The stationary phase consists of a nonpolar silica gel modified by C8 or C18 covalently bonded alkyl chains. In LC-MS, the exposure of lipids to oxygen is minimized, which reduces the possibility of auto-oxidation. Notable is also that LC-MS has a good reproducibility by reducing artifacts appearing in TLC separation techniques (Pulfer and Murphy, 2003).

2.1.3 Mass spectrometry

The success of mass spectrometry in lipidomics attributes to its high sensitivity and high specificity (mass resolution). High-resolution mass spectrometry aids in identification of ions through the mass to charge ratio (m/z), which provides information about the elemental composition. Further fragmentation of the ion gives insights into structural buildup. Thus, not only differentiation between lipids with similar mass can be achieved but also discrimination between isomeric (different structure but same chemical formula) and isobaric species (species with the same mass) (Wenk, 2010).

The mass spectrometer basically consists of an ion source, producing gaseous ions, the mass analyzer, for separation of ions according to their mass to charge ratio (m/z) and subsequently the detector to measure the ion current. The development of soft ionization techniques such as electro-spray ionization (ESI) or matrix-assisted laser desorption ionization (MALDI) in combination with mass spectrometry enables a

rapid and sensitive analysis of lipids. Especially ESI has a high popularity and wide application in lipidomics (Murphy and Nicolaou, 2013). In electro-spray ionization, an electric field is applied between the capillary and the inlet of the mass spectrometer to induce charge accumulation to a liquid, passing through a capillary tube. A spray of small and highly charged particles is formed, which are desolvated by the temperature in the ion source and the applied nitrogen steam. The evaporation of the solvent molecule causes shrinking of the droplet until the Rayleigh stability limit is exceeded. The droplet explodes due to repulsion of congeneric charges into smaller droplets (Coulomb explosion). This process is repeated until the solvent is evaporated and the analyte has been effectively ionized (Han and Gross, 2003; Smith et al., 1990).

Application of ESI-MS can be divided into shotgun lipidomics and LC-coupled approaches (Hu et al., 2009). In mass spectrometry-based shotgun lipidomics, the lipid extract is directly injected into the MS, without any prior chromatographic separation or fractionation prior to the ionization process. Therefore, it provides high-throughput of biological samples and a comprehensive, quantitative analysis of phospho- and neutral lipids as well as sphingolipids and sterols in a single experiment (Ejsing et al., 2009; Guan et al., 2009). Lipids can be identified by the approach of specific fragmentation patterns by neutral loss scanning, precursor ion scanning and product scanning. However, shotgun lipidomics is limited by the low resolution of isobaric lipids without MS/MS experiments and the ion suppression effect for low abundant lipids. These limitations can be avoided by the application of chromatographic separation and subsequent MS detection. Due to prior separation of lipids by RPLC or NPLC the number of competing analytes, passing the MS ion source simultaneously, is reduced. Additionally, to each peak in the chromatogram a characteristic retention time and m/z value can be assigned and guarantees the consistency of quantitative and qualitative results (Hu et al., 2009). In both cases, a huge set of data is generated, which requires suitable software to simplify the data analysis. Different software solutions for distinct MS methods are reviewed in the literature (Katajamaa and Oresic, 2007; Köfeler et al., 2012).

2.2 Lipidomics to study lipid-associated disorders

Lipids play a significant role in cellular signaling, trafficking, membrane structure and energy storage. Thus, they influence numerous important metabolic and signaling

pathways within the cell (Vihervaara et al., 2013). Alterations in lipid homeostasis lead to lifestyle-related diseases. Progress in the field of lipidomics enables detailed profiling of lipid species that serve as potential biomarkers in lipid-associated disorders such as obesity, diabetes, cardiovascular diseases, cancer, and diseases of the central nervous system (CNS) (Murphy and Nicolaou, 2013). Lipids are of high interest when studying obesity, which is caused by “over-nutrition” and imbalanced uptake of energy metabolites (Hu et al., 2009). Characteristic attributes in abdominal obesity are largely increased levels of low-density lipoprotein (LDL) and TAG, and reduced levels of high-density lipoprotein (HDL) in the serum (Pietiläinen et al., 2007). The alteration of serum lipids is mainly provoked by changes in the particular fatty acid distribution of lipid species, which fulfill a certain biological function (Choy et. al., 2004). A link between cancer and altered lipid profiles could be shown in lipidomics studies, where increased levels of lysophospholipids (lyso-PLs) could be detected in the plasma of ovarian cancer patients compared to controls of healthy patients (Xiao et al., 2001). Lyso-PLs operate as cell signaling molecules as well as precursors and intermediates of phospholipid synthesis (Moonlenaar, 1997). Developments in the field of ESI-MS made it possible to detect three different classes of lysophosphatidic acid (LPA) such as acyl-, alkyl-, and alkenyl-LPA. The different subclasses arise from the different chemical linkages of the acyl-chain and the glycerol backbone at the *sn-1* position. Total acyl-, alkyl-, and alkenyl-LPAs are potential targets to distinguish malignant from nonmalignant ascites, because significantly increased levels of LPAs are found in malignant ascites. Furthermore, elevated plasma lysophosphatidylinositol (LPI) levels are potentially prognostic markers for early detection and progression of cancer, e.g. in Stage I ovarian cancer. Therefore, high levels of bioactive lipids may represent prognostic markers to determine tumor progression (Xiao et al., 2001). Other applications of lipidomics to identify biomarkers in lipid-related diseases are in the field of diabetes (Han et al., 2007; Wang et al., 2005), cardiovascular disease (Brindle et al., 2002), inflammation (Fuchs et al., 2005; Jia et al., 2007) and genetic diseases (Fujiwaki et al., 2002; Fuller et al., 2005; Valianpour et al., 2002).

2.3 Flux lipidomics to study lipid dynamics

Flux lipidomics allows to study dynamics of the lipid metabolism and provide insights into synthesis and turnover of lipids over time. Additionally, labeling techniques

enable the tracking of fatty acid incorporation into lipid species. Hence, *de novo* synthesized lipids can be distinguished from total lipids (Li et al., 2013). Several labeling strategies have been applied in the last decade, ranging from radiolabeling to stable isotope labeling. However, stable isotope labeling became the method of choice as it is easier to handle and non-toxic compared to radioactive methods. To study metabolic pathways, the stable isotope is introduced into the system, usually via supplementation to the growth media and serves as precursor to assemble the molecule of interest. Isotopes have the same chemical properties as their corresponding atom but have different masses, by which they can be distinguished by MS (Borén et al., 2012). Basically, every lipid precursor, which provides stable isotope enrichment and forms characteristic fragments of the investigated lipid product, can be used. Deuterium-labeled choline (methyl-D_9-choline), or methionine (methyl-D_3-L-methionine are of common use to elucidate PC metabolism (Boumann et al., 2003; De Smet et al., 2013). Moreover, S(methyl-D_3)adenosyl-L-methionine is used to study the contribution of the PE-N-methylation pathway to PC synthesis (Boumann et al., 2004). D_4-ethanolamine and D_3-serine are utilized to unravel the molecular specificity of PE synthesis and turnover by distinct pathways (Bleijerveld et al., 2007). A further application is to supply labeled fatty acids to the growth media, e.g. U-^{13}C-palmitate for mapping of dynamics in lipid metabolism. However, covering the entire dynamics of lipids is still a challenge. The introduction of stable isotope-labeled substrates into experimental settings complicates the analysis of raw data obtained from MS-based measurements (Li et al., 2013). The application of labeled fatty acids lacks information about endogenous acyl-chain synthesis and may mask several important pathways. Another confinement are the high costs of pulse-labeling experiments due to the large number of isotope labels required. Therefore, further improvements are necessary to determine the substrate selectivity of individual biosynthetic enzymes, to monitor remodeling kinetics and to gain valuable insights into the dynamics of lipid metabolism.

3 Aim

Lipidomic studies in combination with stable isotope labeling shed light on functions and mechanisms of lipids in biochemical processes. However, covering the complete dynamics of lipid networks is still a challenge. The correlation between altered lipid metabolism and progression of lipid-related disorders motivated us to study its regulation and the specific roles of lipids in health and disease.

This study focuses on the establishment of a novel labeling method to unravel how the flux of *de novo* produced fatty acids is controlled in yeast, especially the regulation of acyl-chain composition in membrane phospholipids. We propose that fatty acids are incorporated into lipid species in a highly coordinated manner by tightly controlled metabolic channeling, including remodeling and re-acylation by substrate-specific acyltransferases. The new technique should be robust, applicable for the whole yeast deletion collection and cheap to measure endogenously synthesized fatty acids. As a proof of concept, this method is applied to study the contribution of i) the glycerol-3-phosphate acyltransferase and ii) the choline-phosphate cytidylyltransferase activity to phospholipid and neutral lipid synthesis and turnover.

4 Results

The goal of this master thesis was the establishment of a new labeling method to study the metabolic fluxes of fatty acids with the help of mass spectrometry. The method was subsequently applied to characterize the lipid composition in the yeast wild type BY4742 and in mutants defective in either glycerol-3-phosphate acyltransferase activity or the Kennedy pathway, to measure the contribution of these pathways to acyl chain remodeling and lipid homeostasis.

4.1 Validation of ^{13}C glucose purity by GC-MS

For our labeling experiment, cells were pre-labeled with ^{13}C glucose to study the incorporation of *de novo* synthesized fatty acids into phospholipids and neutral lipids. Therefore, we first checked whether the purchased ^{13}C glucose consisted solely of ^{13}C carbon atoms. To this end, trimethylsilyl ethers of α-D-glucose were prepared, purified by gas chromatography (Sweeley et al., 1963) and analyzed by mass spectrometry. According to DeJongh et al. 1969, the characteristic ion fragments from the mass spectra could be assigned to their elemental composition. A selection of fragments (m/z 435, 361 and 345), which show a stepwise elimination of trimethylsilanol or loss of trimethylsilyloxy radical and trimethylsilanol from the molecular ion, have been chosen to compare the ion fragments of ^{12}C glucose to ^{13}C glucose. The observation showed a carbon specific mass offset of solely m/z +6 in ^{13}C glucose, which confirmed a complete labeling of ^{13}C glucose (Figure 6).

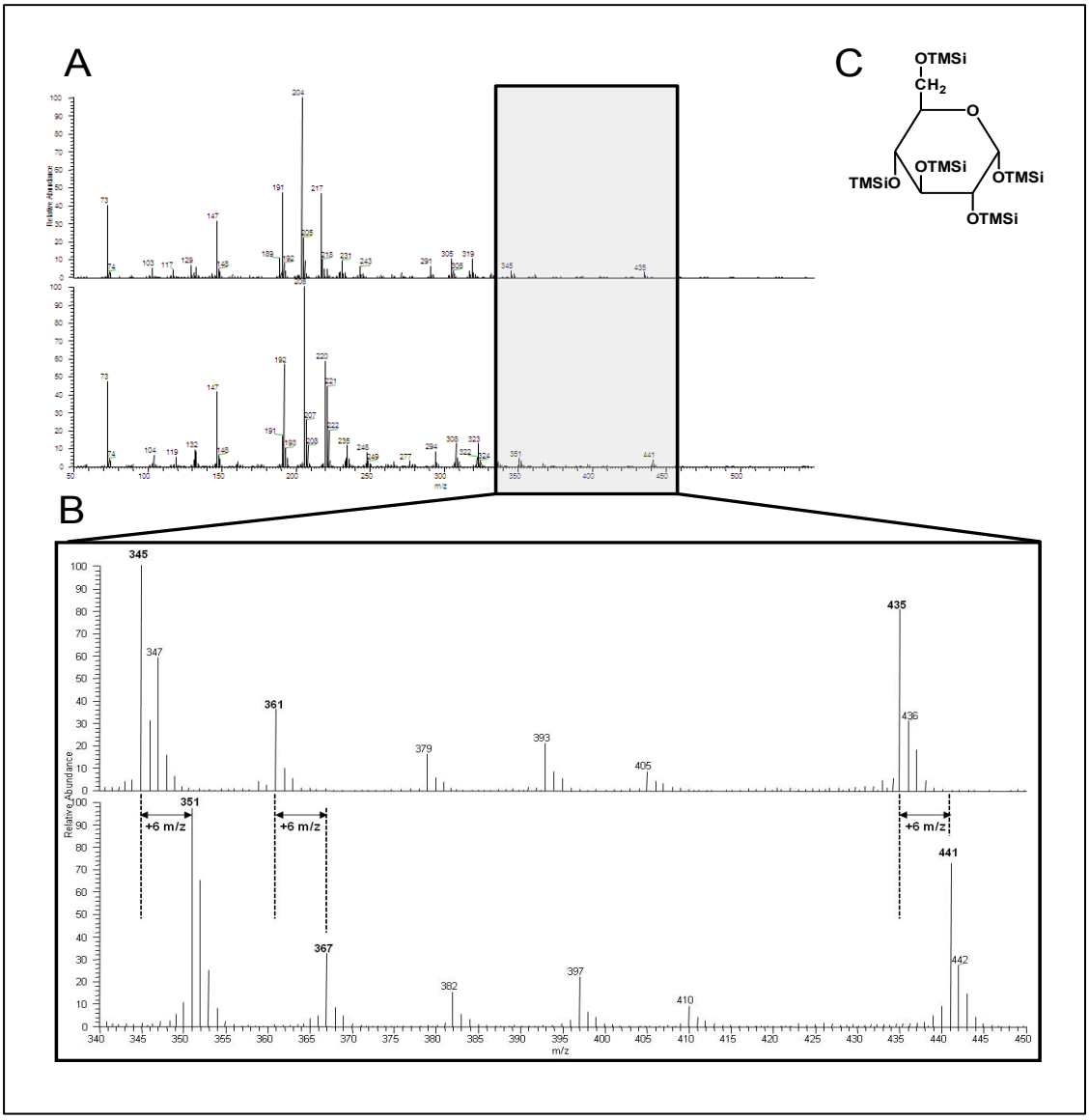

Figure 6: Glucose derivatization and fragmentation. (A) 70-eV mass spectrum of ^{12}C (upper panel) and ^{13}C (lower panel) 1,2,3,4,6-penta-O-trimethylsilyl-α-D-glucopyranose. The following characteristic fragments (B) are used to show the mass offset of m/z +6 in ^{13}C glucose compared to ^{12}C glucose: m/z 435 - TMSiOH - CH_3; m/z 345 - 2 TMSiOH - CH_3; m/z 361 - TMSiOH - TMSiO. This observation indicates a complete labeling of ^{13}C glucose. (C) Structural formula of 1,2,3,4,6-penta-O-trimethylsilyl-α-D-glucopyranose.

4.2 Mass tag strategy to monitor *de novo* synthesized lipid species

Stable isotopic labeling in combination with mass spectrometry are widely used and suitable methods to monitor the flux of fatty acids in total lipid extracts. However, most of these techniques are established as pulse labeling experiments to visualize the fluxes of distinct metabolites. We report a novel method for monitoring phospholipid and neutral lipid species in total lipid extracts. The method employs a

specific "mass-tag" strategy by pre-cultivation of cells in ^{13}C glucose to generate fully labeled lipid species with carbon-specific mass offsets ("steady-state").

4.2.1 ^{13}C incorporation in steady state-labeled cells

To simplify the proof of principle, phosphatidylcholine PC 32:2 was taken as an example to show that the ^{12}C carbon atoms incorporated into the two fatty acids in *sn-1* and *sn-2* position as well as the 3 carbon atoms in the glycerol backbone are replaced by ^{13}C carbon atoms (Figure 7A). This isotopic exchange leads to an increase of m/z +35 in this particular case. Subsequent shifting of cells to media containing ^{12}C glucose ("chase" conditions) enabled to study recovery rates of *de novo* synthesized lipid species by mass spectrometry by the appearance of non-labeled lipid species over time (Figure 7B).

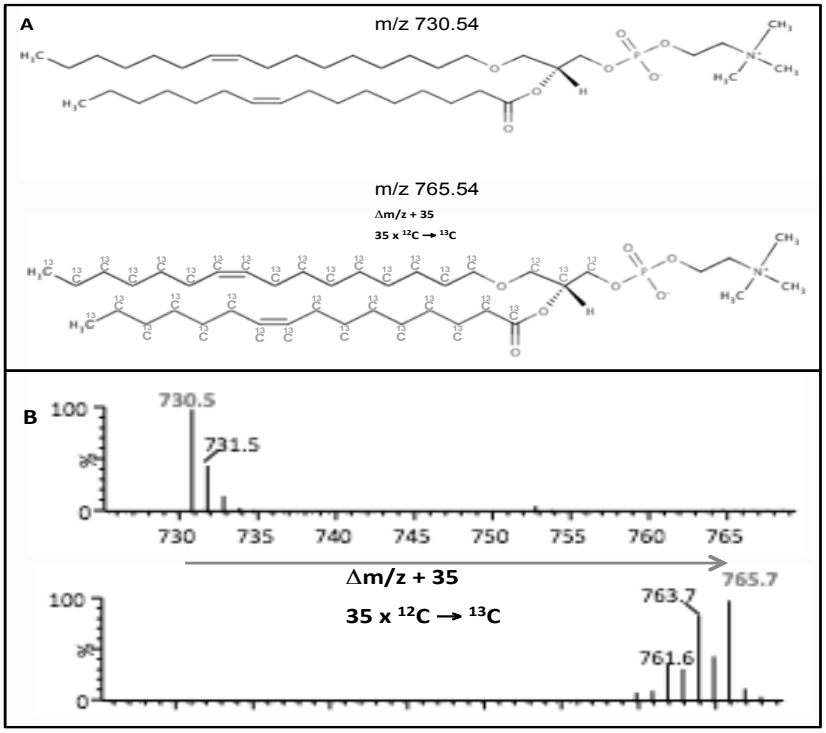

Figure 7: Mass-tag strategy. (A) Phosphatidylcholine PC 32:2 has a mass to charge ratio of m/z 730.54. ^{13}C carbon atoms can be incorporated into *de novo* synthesized fatty acids and the glycerol backbone. (B) Carbon specific mass offset due to ^{13}C labeling. A qTOF-MS full ion scan of a PC 32:2 shows a mass offset of m/z +35 from 730.5 (unlabeled cells, upper panel) to 765.7 (fully-labeled cells, lower panel).

4.2.2 The phospholipid head group remains unlabeled in ^{13}C glucose containing media

The phosphate head group specifies the class of a phospholipid and is esterified on the *sn-3* position of the glycerol backbone. A limitation by applying this method on the amino acid auxotroph BY series is the inability to label the head group of phospholipids. To verify that only the head group remained unlabeled and no other semi-labeled species appeared during growth, further fragmentations of the molecular ion were executed. The phosphocholine head group of PC was detected in an MS/MS experiment as a characteristic ion at m/z of 184.08 in both labeled and unlabeled cells. This observation proves that the head group was unlabeled, because no mass shift was detected (Figure 8A). The MS/MS experiment of PE 34:2 shows a neutral loss of phosphoethanolamine at a Δ m/z of -141. This specific mass loss appeared under both ^{12}C and ^{13}C conditions, corresponding to an unlabeled PE head group (Figure 8B).

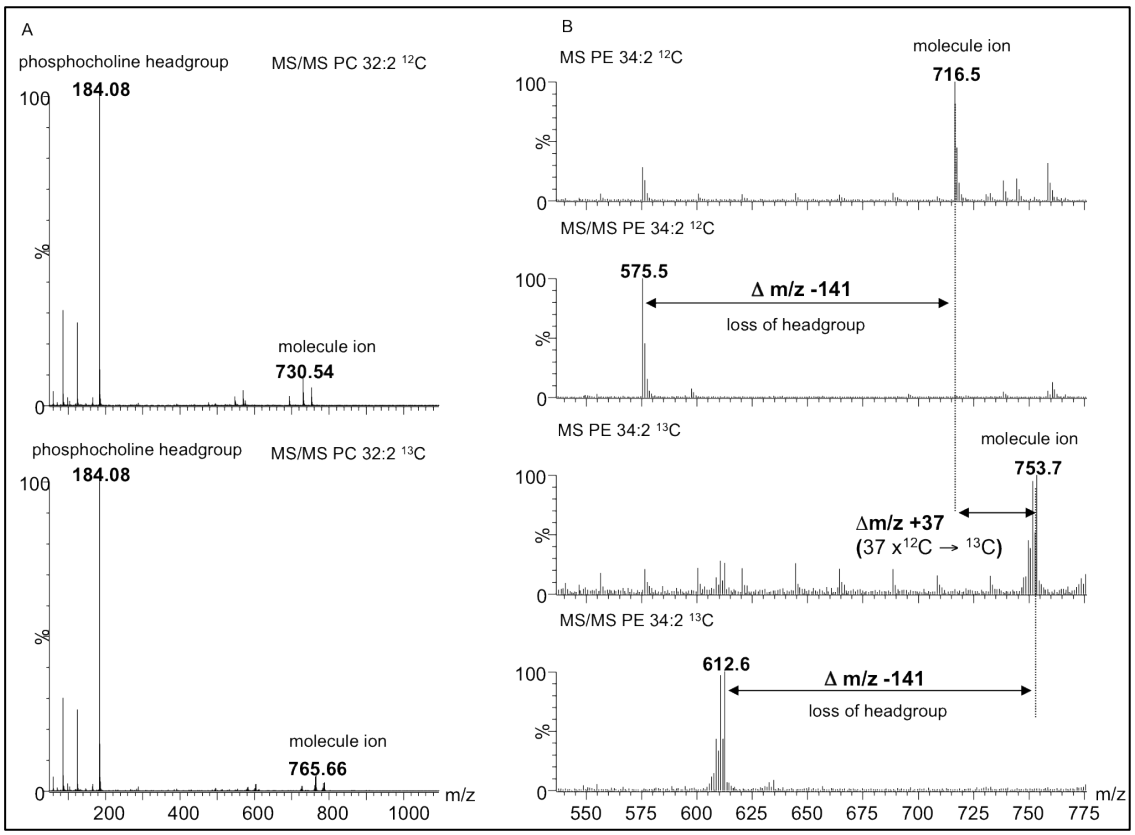

Figure 8: Unlabeled head group due to amino acid supply in the growth media. (A) The chromatogram and spectrum of PC 32:2 show a further fragmentation of the molecule ion (MS/MS experiment). In the full ion scan, phosphocholine is detected at m/z 184.08 under both ^{12}C and ^{13}C glucose conditions, corresponding to an unlabeled head group. (B) Spectra of MS/MS experiments of PE 34:2 show a neutral mass loss of Δ m/z -141 for phosphoethanolamine in labeled and unlabeled cells, respectively, monitoring an unlabeled head group.

4.2.3 Mass tag strategy to reveal dynamics in lipid metabolism

Stable isotopic labeling techniques in combination with time resolved analyses are described in only a view studies (Pynn et al., 2011). To determine the kinetics of phospholipids and TAG in the lipid metabolism of the wild type BY4742, the mass-tag strategy in combination with an UPLC-qTOF method (Knittelfelder et al., 2014) was used to analyze levels of lipids at different times of growth. Wild type cells were pre-cultivated in ^{13}C glucose medium (steady state cells/ or time point zero) and transferred to fresh medium containing ^{12}C glucose. As a control, cells were also pre-cultivated and analyzed in ^{12}C glucose (unlabeled cells). At indicated time points of growth, samples were collected and the total lipid extracts were analyzed with UPLC-qTOF in positive ionization mode (ESI^+). Figure 9A compares chromatograms of labeled cells (upper panel) and unlabeled cells (lower panel). The analysis illustrates that the same lipid species appeared at the identical retention times, independent on their labeling state. Taking PC 32:2 and PC 34:2 as examples, they both appeared at 14.89 and 16.88 minutes, respectively, in labeled and unlabeled cells. The full scan spectrum shows unlabeled PC 32:2 and 34:2 at m/z 730.55 and m/z 758.57, respectively. Due to the possibility to incorporate ^{13}C carbon atoms into two fatty acids and the glycerol backbone, a mass offset of m/z +35 for PC 32:2 and m/z +37 for PC 34:2 can be reached, which is mirrored in the mass shift to m/z 765.65 and 795.69, respectively. The upper panel of the spectrum shows fully labeled PC 32:2 at time point zero with m/z 765.66. However, the observation also revealed peaks with a mass offset of m/z +33 and m/z +31, indicating 2 or 4 non-labeled carbon atoms in the backbone. This effect could arise through synthesis of acetyl-CoA out of the supplied unlabeled amino acids in the growth media.

After shifting cells back to ^{12}C glucose, semi-labeled PC 32:2 appeared primarily at m/z 749.60 and m/z 746.59 indicating an incorporation of *de novo* synthesized fatty acids into already existing ^{13}C labeled lyso-PC species. The same observations were made for PC 34:2, for which peaks at m/z 777.64 and m/z 779.63 could be detected. After 7 hours, only unlabeled PC 32:2 and PC 34:2 species were detected. This examination is in line with the unlabeled control cells, shown in the bottom panel of the spectrum (Figure 9B).

However, from this analysis it was unclear, whether the semi-labeled species were products of one fatty acid exchange or if two semi-labeled fatty acids were incorporated. Therefore, MS/MS experiments in negative ionization mode (ESI^-) were performed. Figure 10 displays the full scan spectrum of PC 34:2 in ESI^- mode. The PC 34:2 appears unlabeled at m/z 802.56. The incorporation of ^{13}C carbon atoms into two fatty acids and the glycerol backbone of PC 34:2 reflects the mass shift to m/z 839.69. Semi-labeled lipid species appeared primarily at m/z 821.63 and m/z 823.63 indicating an incorporation of *de novo* synthesized C16 or C18 fatty acids.

The corresponding MS/MS analysis, which was performed to further fragment the molecular ions, showed palmitoleic acid (16:1) at m/z 269.27 and oleic acid (18:1) at m/z 299.31 in fully labeled cells bearing a mass offset from the unlabeled fatty acids of m/z +16 and m/z +18, respectively. Again, mass offsets with m/z +14 for palmitoleic acid and m/z +16 for oleic acid appeared, indicating the presence of 2 non-labeled carbon atoms in the fatty acid. After shifting cells back to ^{12}C glucose containing media, mass losses of m/z -16 for palmitoleic acid and m/z -18 for oleic acid were detected and no peaks appeared between these mass shifts. This proves that an existing labeled fatty acid was replaced by an unlabeled *de novo* synthesized fatty acid and no semi-labeled fatty acids were reacylated in lyso-PC. The peak at m/z 255.22 can be explained as a 16:0 fatty acid belonging to PE 32:1, which is detected at the same retention time as PC 34:2, rather than a 16:1 fatty acid with 2 remaining labeled carbon atoms, as this pattern is not observed for the oleic acid peak at m/z 281.

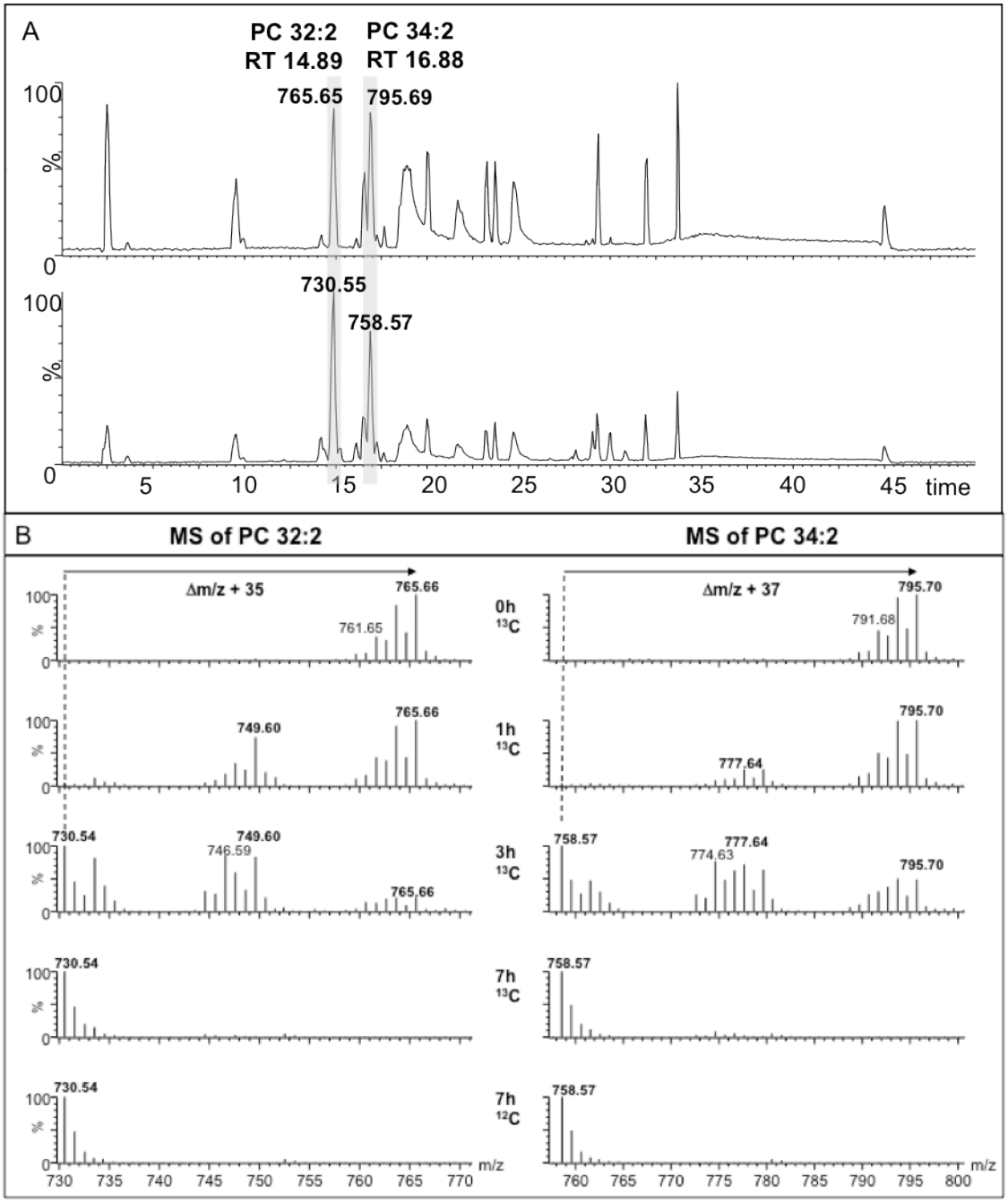

Figure 9: (A) Chromatogram of lipids after UPLC separation shows identical retention times for equal lipid species independent on labeling state. (B) MS spectra of PC 32:2 and PC 34:2 at different times of growth (pulse labeled steady state cells at 0 hours, cells 1, 3 and 7 hours after chase conditions and unlabeled control cells). See text for details.

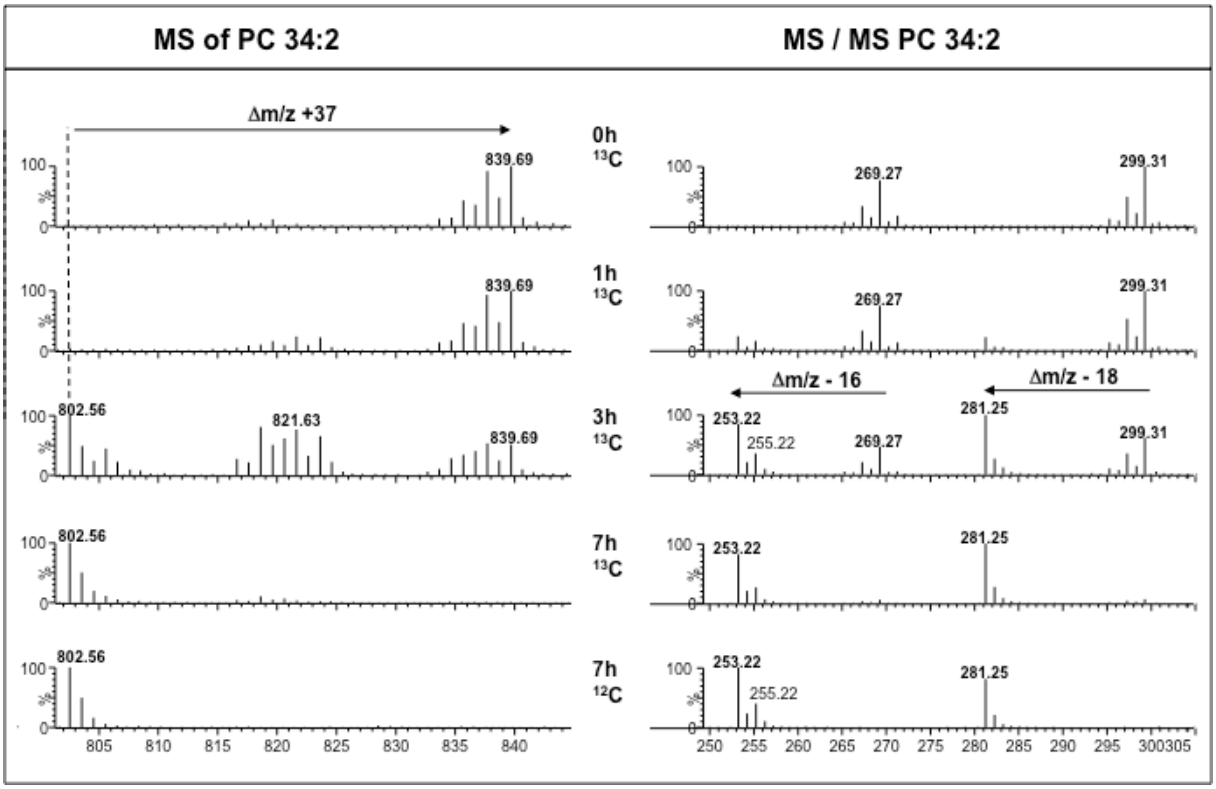

Figure 10: Remodeling kinetics in the lipid metabolism. MS spectrum of a phosphatidylcholine PC 34:2 molecular ion in ESI$^-$ mode at distinct times of growth. 0 hour time point shows fully ^{13}C labeled steady state cells. Subsequent shifting to ^{12}C glucose containing media produce semi-labeled intermediates at time points 1 hour and 3 hour. Fully unlabeled cells at time point 7 hours, showed the same spectrum as unlabeled ^{12}C control cells grown under the same conditions. The corresponding MS/MS spectrum shows palmitoleic acid and oleic acid during growth in chase conditions. See text for details.

4.3 *In vivo* dynamics in lipid metabolism of wild type yeast

To ensure that differences in lipid profiles are not attributed to different growth of cells, we determined growth curves by measuring optical density at 600 nm (OD_{600}) at distinct time points: 0,1,3,5 and 7 hours in ^{13}C glucose pre-labeled cells and unlabeled control cells, which were cultivated in the same way as labeled cells. The growth curves showed a lag phase, which occurred after shifting cells to fresh ^{12}C glucose containing media. Due to the fact that cells were pre-labeled with ^{13}C glucose to steady state levels, cells reached a late logarithmic growth phase and therefore this effect appeared. The doubling time was calculated as described in *Materials and Methods* from 1-7 hours and showed comparable growth behaviors independent of labeled or unlabeled glucose, as expected (Figure 11).

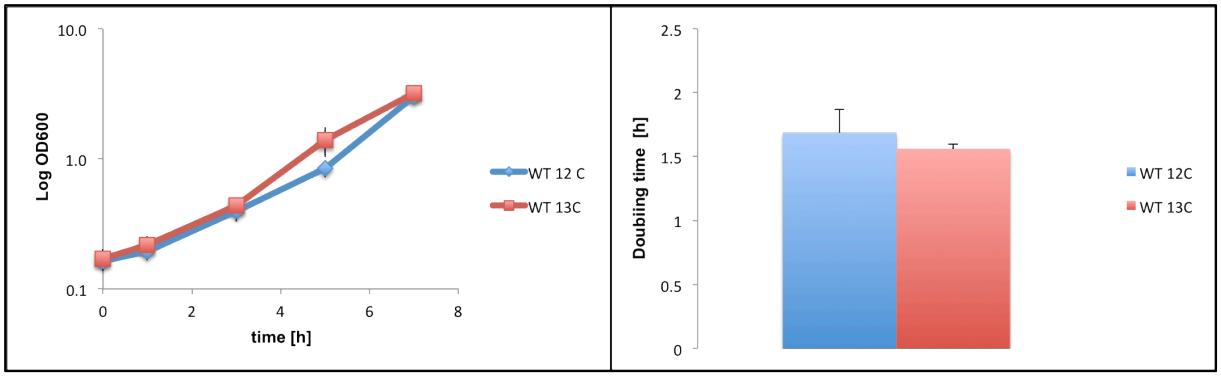

Figure 11: Growth curves and doubling times of the wild type BY4742 under ^{13}C and ^{12}C glucose conditions show comparable growth behavior.

4.3.1 Kinetics of phospholipid acylation in wild type BY4742 shows almost full exchange of ^{13}C-carbon atoms with ^{12}C-carbon atoms within 7 hours

Data obtained from the UPLC-qTOF analysis was processed with the program Lipid Data Analyzer (Hartler et al., 2011). To this end, an excel file was used, which included the retention times and m/z ratios of the ^{12}C lipid species. The analysis provided the molecular mass of each individual lipid species with corresponding peak area at indicated time points. Figure 12 shows the glycerolipid profiles (PE, PC, DAG, TAG and PI) of labeled and unlabeled control cells. Labeled cells were used to study *de novo* synthesized lipids and unlabeled control cells to show the total lipid profile over time. In unlabeled cells, a drop in TAG levels was detected in the first hours after shifting cells to ^{12}C glucose media. This finding is in correlation with the literature and occurs because lipolysis takes place when cells enter logarithmic growth. Additionally PE levels increased over time and peaked at the 3 hours time point in control cells, whereas PC and PI levels remained constant until the 5 hours time point. However, in the late logarithmic phase, PE, PC, PI and DAG levels decreased and TAG levels increased, again consistent with previous studies (Klose et al., 2012). At the 0 hour time point, labeled lipid species extracted from cells following ^{13}C glucose pre-cultivation could not be detected, indicating the steady state incorporation of ^{13}C carbon atoms into all analyzed lipid species. The kinetics profiles over time of labeled cells displayed a lag phase, which is in line with the observed lag phase in growth. Another reason for this delay might be that ^{13}C carbon atoms are still present in the metabolism and therefore, it takes up to 1 hour to substantially incorporate ^{12}C carbon atoms into lipid species to reach the lower

detection limit of the mass spectrometer. By comparing the diagrams, *de novo* synthesized DAG species showed a sigmoid curve progression and reached the saturation level already at the 3 hours time point, whereas PC and TAG levels increased continuously during the analyzed 7 hours. Most notable is the fast *de novo* synthesis observed in PI species compared to the other analyzed lipid classes, indicating a rapid exchange of FA in PI in the presence of inositol in the growth media (Figure 13). Taken together, these data show that *de novo* synthesis of PI is faster than of other lipid classes, as the comparison of labeled versus unlabeled cells at 5 hours of growth under chase conditions showed a full exchange of ^{13}C carbon atoms with ^{12}C carbon atoms in PI species. In all other analyzed lipid classes, an almost full exchange was observed at 7 hours of growth.

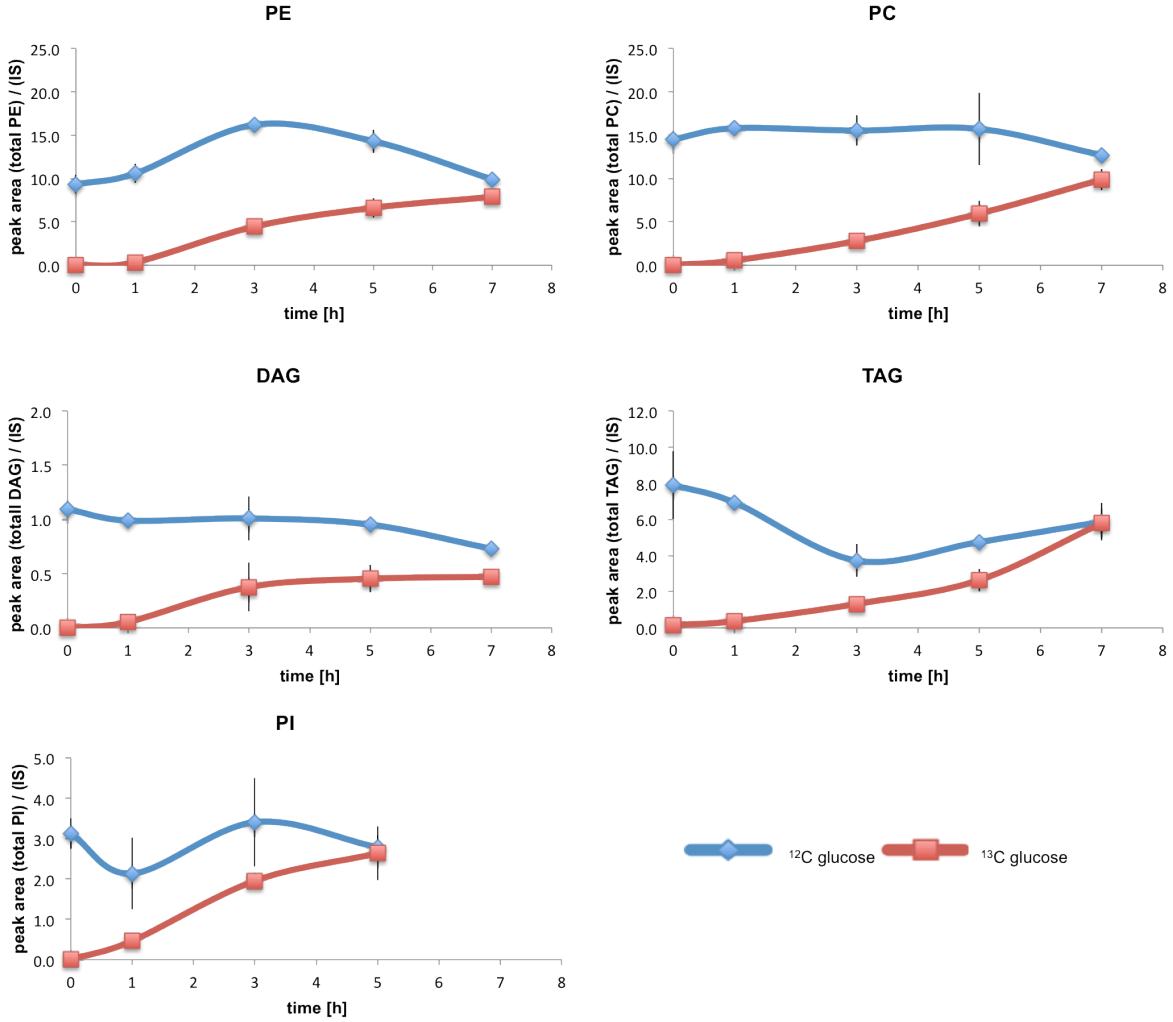

Figure 12: Lipid profiles of wild type BY4742 shows PE, PC, PI, DAG and TAG species. Cells were grown to late-logarithmic phase for 16 hours (time point zero) in medium with ^{13}C glucose and shifted to fresh medium containing ^{12}C glucose (red line). Control cells were pre-cultivated in medium containing ^{12}C glucose and shifted to fresh medium containing ^{12}C glucose (blue line). At indicated time points (0, 1, 3, 5 and 7 hours) cells were harvested and subjected to lipid extraction. The total lipid extract was analyzed with a UPLC-qTOF system as described above.

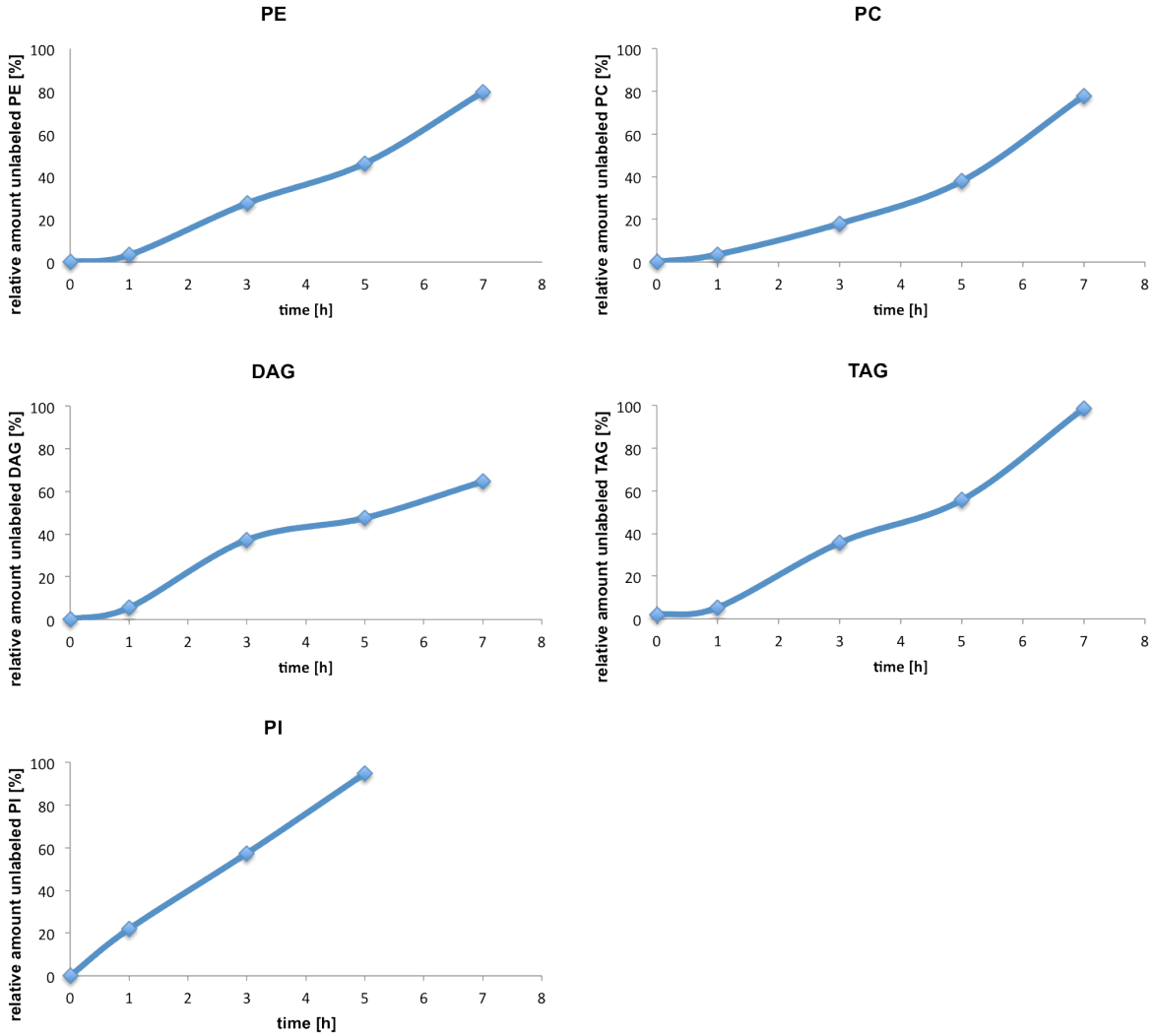

Figure 13: Relative amount of unlabeled species illustrating the proportion of *de novo* synthesized versus steady state levels of lipid species. This observation shows that the exchange of fatty acids is 2-3 times faster in PI than in PE and PC.

At time point 5 hours, both ^{12}C and ^{13}C carbon atoms are found in lipid species in pre-labeled cells. Therefore, we chose this time point to compare the fatty acid composition with that of unlabeled cells using gas chromatography coupled to a flame ionization detector (GC-FID). Figure 14 shows a comparable fatty acid composition in labeled and unlabeled control cells, further validating the established method.

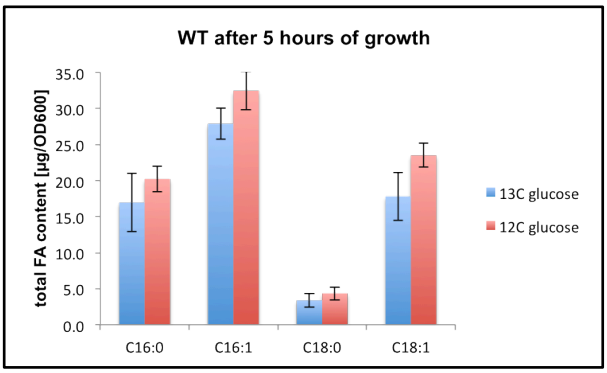

Figure 14: GC-FID analysis of labeled and unlabeled wild type cells at 5 hours of growth displays comparable FA compositions.

4.3.2 The phospholipid acyl-chain composition changes over time from mono- to di-unsaturated species

When investigating the profile of *de novo* synthesized PE species, we observed that the mono-unsaturated species PE 32:1 and PE 34:1 showed the fastest recovery rates under chase conditions (Figure 15). However, this pattern changed over time as the mono-unsaturated species decreased and the di-unsaturated species increased. The levels at 7 hours were very similar compared to the pattern of the unlabeled control cells (data not shown).

The acyl-composition of *de novo* built-up PCs showed a different profile over time; the mono-unsaturated PC 32:1 was synthesized very rapidly compared to the other species but after the first 3 hours, the lipid profile shifted from mono-unsaturated to di-unsaturated phospholipids, again matching the profile of the control cells. These observations indicate that saturated (and probably shorter chain) fatty acids are synthesized and incorporated faster into lipid species in the first hours but are exchanged afterwards by unsaturated (and longer chain) fatty acids

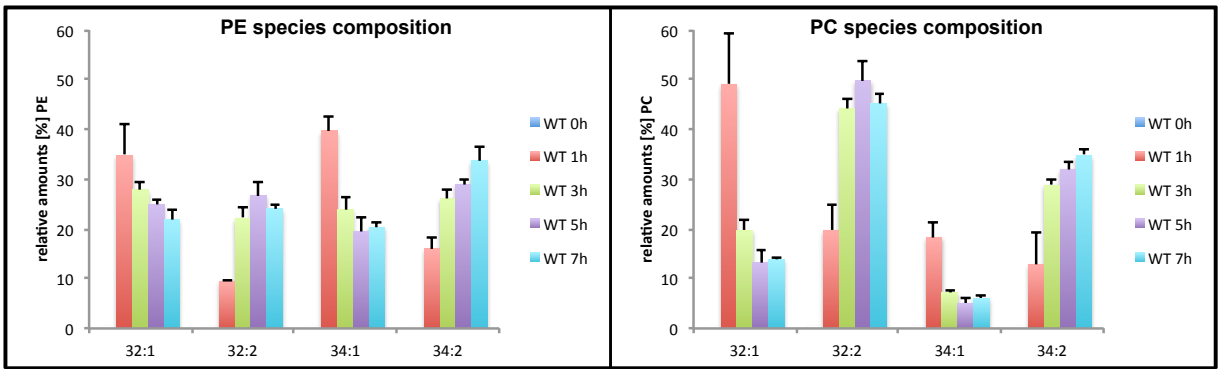

Figure 15: Relative amounts of *de novo* synthesized PC and PE lipid species in BY4742 WT cells at distinct time points. The lipid composition changes over time from mono- to di-unsaturated phospholipid species.

4.3.3 Detection of remodeling kinetics in phospholipids

To gain further insights into the kinetics of lipid remodeling, the mass list for data analysis was extended for the additional detection of fully ^{13}C labeled lipid species and semi-labeled intermediates. We concentrated on the four predominant PC species in yeast: di-unsaturated 32:2 (containing two C16:1 acyl-chains) and 34:2 (containing one C16:1 and one C18:1 acyl-chain), and the mono-unsaturated species 32:1 (composed of C16:0 and C16:1) and 34:1 (composed of C16:0 and C18:1 and / or of C16:1 and C18:0). In semi-labeled species, a fully labeled acyl-chain was replaced by a completely unlabeled acyl-chain (as confirmed with MS/MS analysis; Figure 10). Hence, the following intermediates could be detected: 19C_32:1 (one 16:0 or 16:1 acyl-chain replaced), 19C_32:2 (one 16:1 acyl-chain replaced), 21C_34:1 (one 16:0 or 16:1 acyl-chain replaced), 21C_34:2 (one 16:1 acyl-chain replaced), 19C 34:1 (one 18:0 or 18:1 acyl-chain replaced) and 19C_34:2 (one 16:1 acyl-chain replaced). The first number indicates the remaining carbon atoms in the distinct lipid species. The extension of the mass list enabled the determination of the decrease in fully labeled phospholipid species and incorporation of unlabeled fatty acids into labeled lysophospholipid species. The upper panel of Figure 15 displays the decrease of fully labeled PC species, also showing that di-unsaturated PC 32:2 was the most abundant species followed by PC 34:2 and mono-unsaturated PC 32:1 and PC 34:1, in steady state labeled cells. Most notably, a rapid decrease of fully labeled species after 1 hour was detected, indicating a fast exchange of fatty acids. These findings are in agreement with the recovery measurements of *de novo* synthesized phospholipids (bottom panel). One has to mention that only the decrease of fully labeled species was monitored as shown in Figure 16, and the m/z -

2 and m/z -4 peaks were not accounted in the calculations, which explains the lower area values in panel A as compared to panel C. To study remodeling kinetics, we had a look at fully labeled species, which had one fatty acid exchanged by an unlabeled *de novo* synthesized fatty acid (Figure 16). After 1h, the first intermediates appeared, indicating faster remodeling kinetics in mono-unsaturated species than in di-unsaturated species: mono-unsaturated species had the highest amounts of intermediates at time point 1 hour, whereas di-unsaturated species peaked at the 3 hour time point. However, the highest intermediate levels were detected for di-unsaturated species. Within 7 hours, all fully labeled species as well as intermediate species vanished and the unlabeled species reached steady state levels as compared to control cells. This leads to the conclusion that *de novo* synthesized saturated fatty acids are incorporated faster into lipids than mono-saturated fatty acids. However, steady state lipid composition was achieved after the initial 3 hours up to 7 hours of growth with regard to the relative distribution pattern.

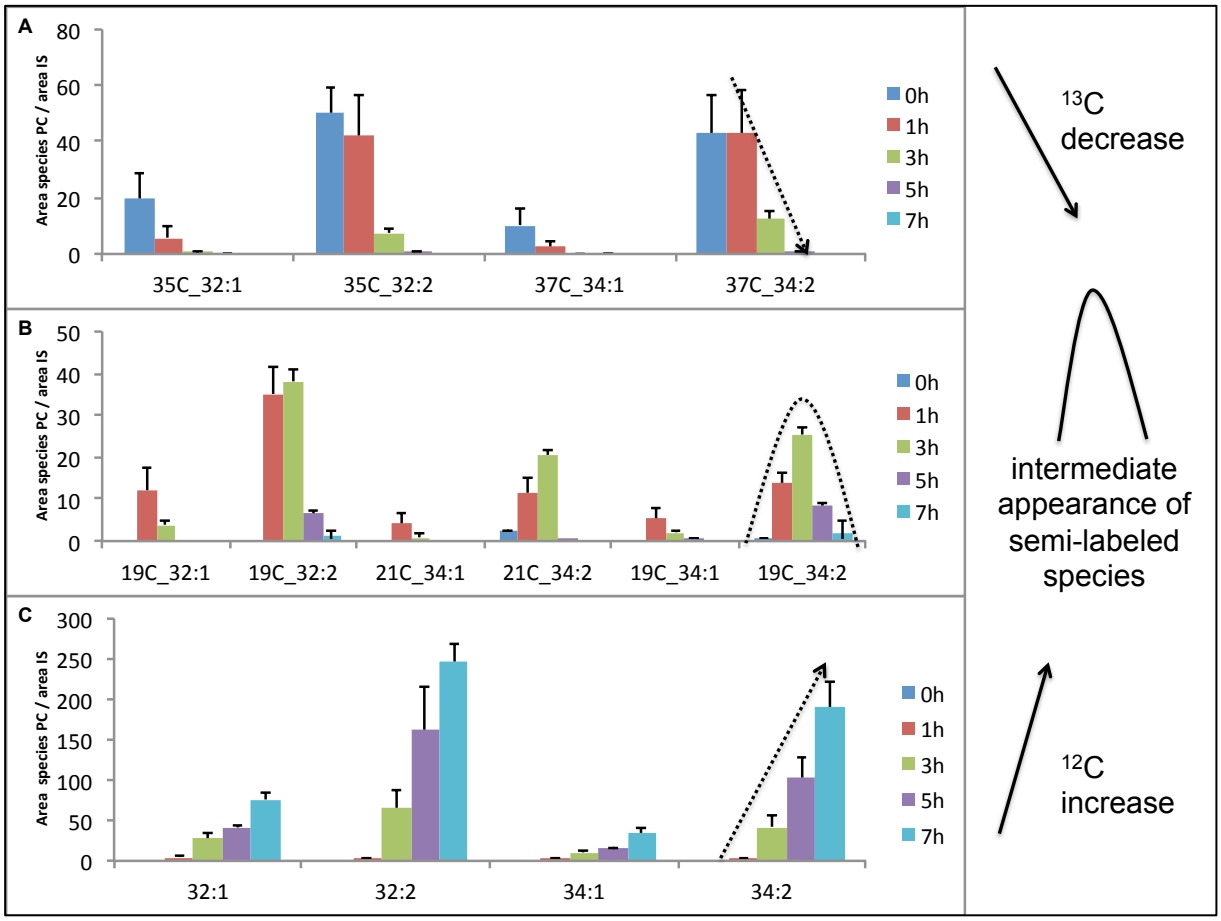

Figure 16: Detection of remodeling kinetics in phospholipids. (A) Decrease of fully labeled PC species. (B) Semi-labeled PC species. (C) Recovery of *de novo* synthesized PC species.

4.4 The contribution of the glycerol-3-phosphate acyltransferase Gpt2 to phospholipid synthesis and turnover

Next, we examined whether there was a change in phospholipid and neutral lipid composition by deleting *GPT2*, the gene encoding glycerol-3-phosphate / dihydroxyacetonephosphate acyltransferase (GPAT). In yeast, two enzymes namely Gpt2 and Sct1 are involved in the first acylation step of glycerol-3-phosphate to produce lysophosphatidic acid (Zheng and Zou, 2001). However, they differentially contribute to lipid synthetic pathways (Zaremberg and McMaster, 2002) and recent studies propose that lipid fluxes are controlled at the GPAT step (Marr et al., 2012). These enzymes show substrate specificity and channel the incorporation of specific fatty acids into lipid species (De Smet et al., 2012). To study the impact of Gpt2 on *de novo* synthesis rates and also remodeling dynamics of lipid species, lipid extracts of the deletion mutant *gpt2* were analyzed by mass spectrometry and compared to wild type. Cells were cultivated as described in *Materials and Methods*. Labeled and unlabeled control cells showed similar growth behavior and doubling times (Figure 17) and were almost identical to wild type (Figure 11).

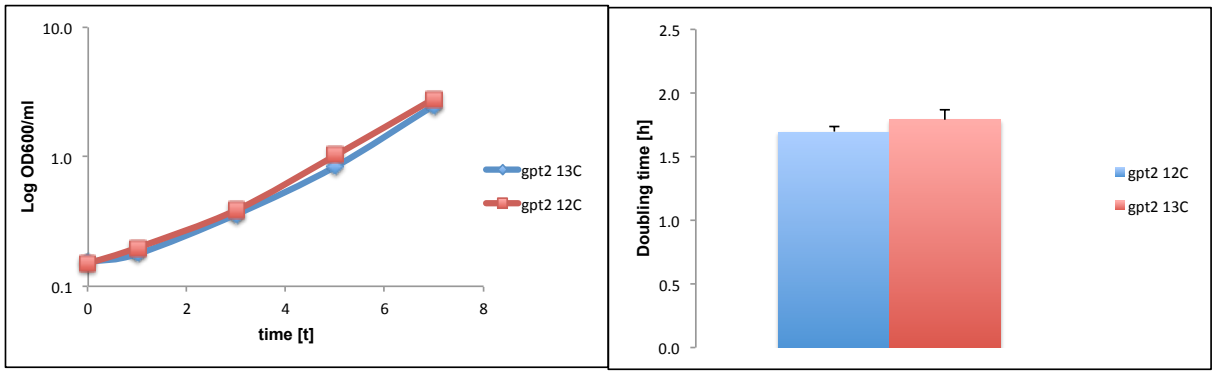

Figure 17: Growth curves and doubling times of the *gpt2* mutant under ^{13}C and ^{12}C glucose conditions show comparable growth behavior.

The lipid profile of *gpt2* (Figure 18) displayed similar kinetics as the wild type. In control cells the lipolysis effect was observed as TAG levels decreased in the first hours and an increase in PE and PI levels and constant PC and DAG levels over time were determined. *De novo* synthesized lipid species increased gradually, whereby PC, PI and TAG levels rose linearly and PE and DAG showed a rather sigmoid curve progression as also observed in wild type (Figure 12). The exchange of ^{13}C carbon by ^{12}C carbon is clearly detectable in PI species at time point 5 hours

and in PE, PC and TAG species at time point 7 hours by reaching the same levels as in control cells.

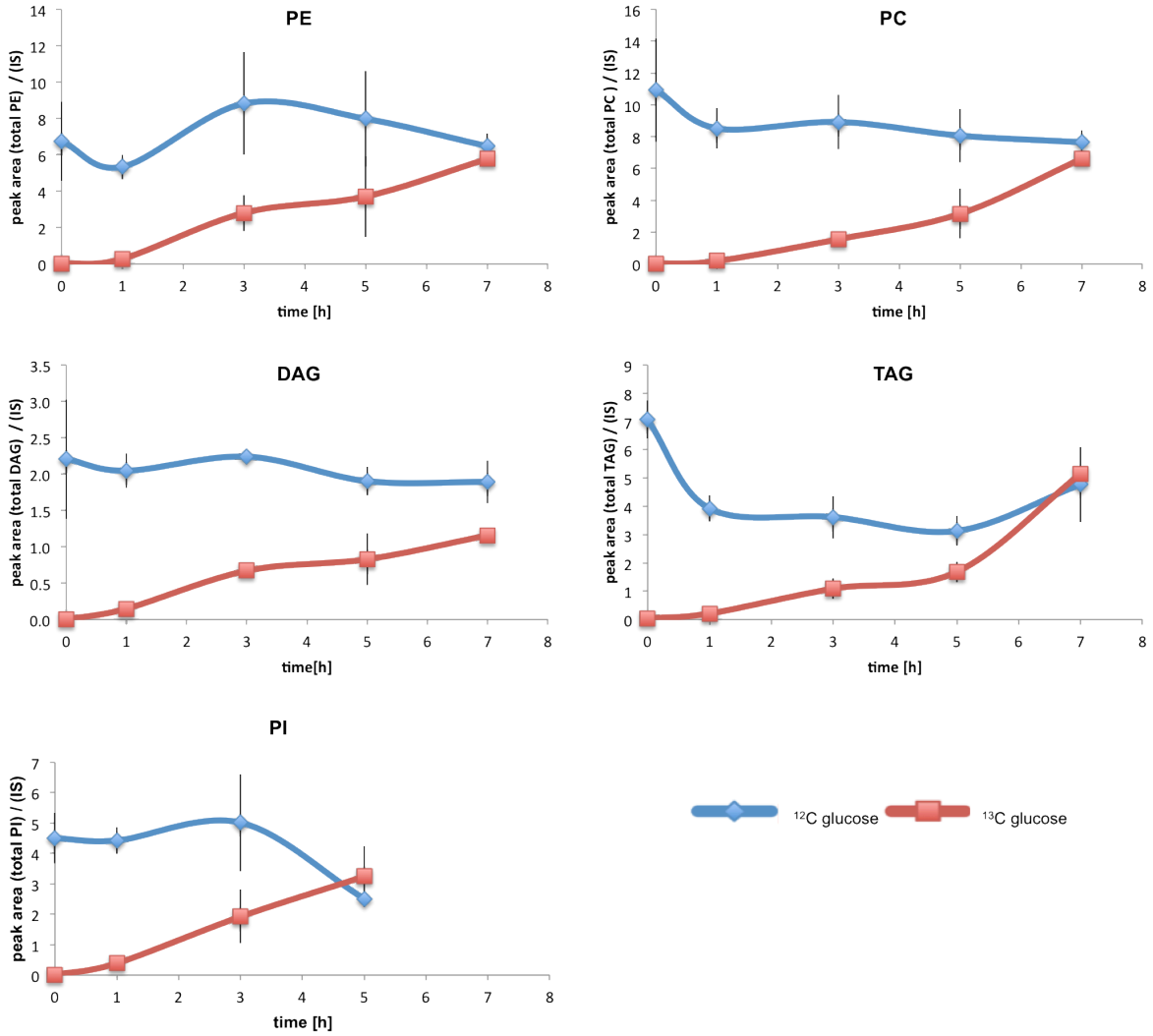

Figure 18: Lipid profile of *gpt2* shows PE, PC, PI, DAG and TAG species. Cells were grown to late-logarithmic phase for 16 hours (time point zero) in medium with ^{13}C glucose and shifted to fresh medium containing ^{12}C glucose. Control cells were pre-cultivated in medium containing ^{12}C glucose and shifted to fresh medium containing ^{12}C glucose. At indicated time points (0, 1, 3, 5 and 7 hours) cells were harvested and subjected to lipid extraction. The total lipid extract was analyzed with a UPLC-qTOF system as described above.

In comparison to the wild type, the *gpt2* mutant showed increased DAG levels and decreased PE and PC levels, indicating a substantial contribution of Gpt2 to phospholipid synthesis (Figure 19).

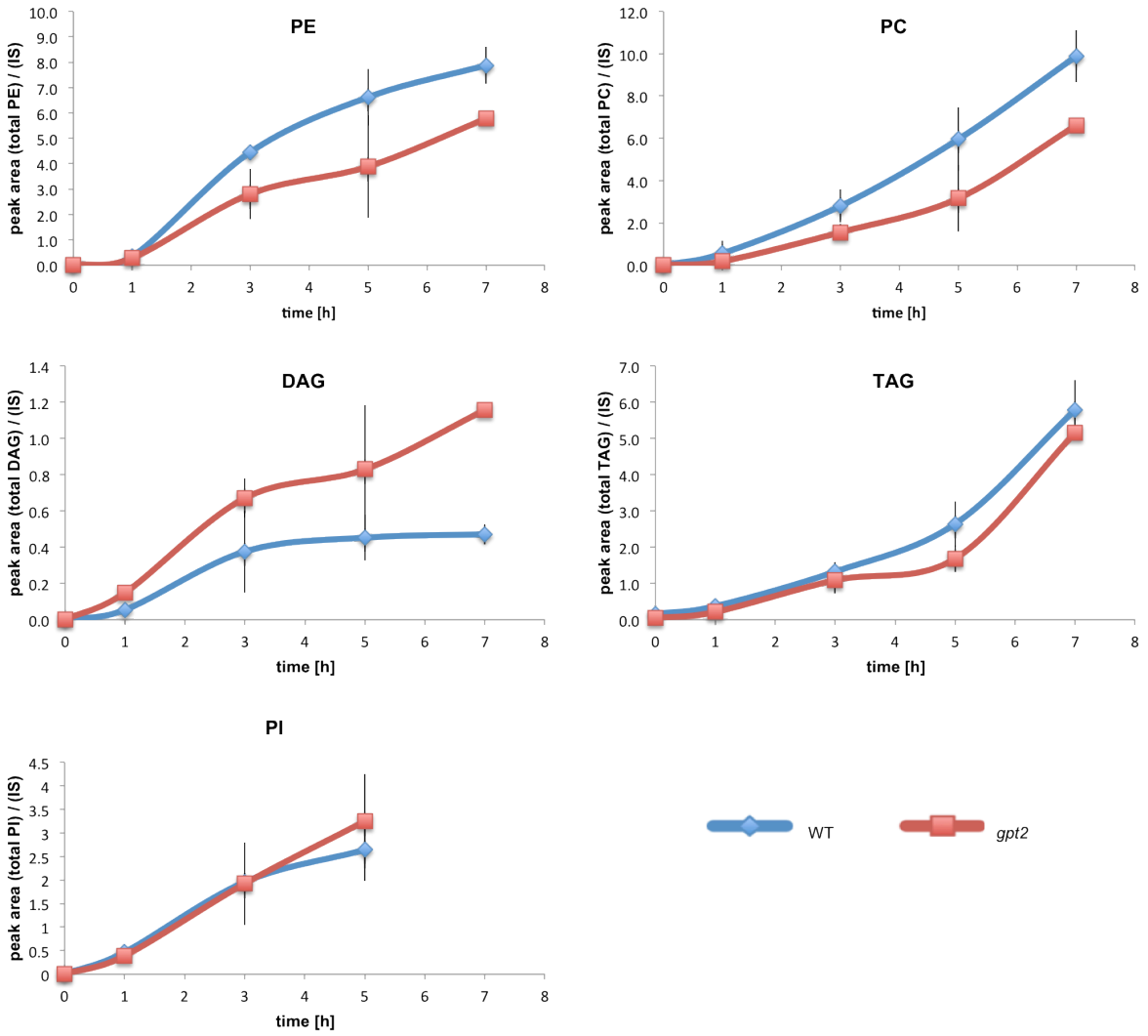

Figure 19: Lipid profile of the *gpt2* mutant compared to wild type show PE, PC, PI, DAG and TAG species. Cells were grown to late-logarithmic phase for 16 hours (time zero) in medium with ^{13}C glucose and shifted to fresh medium containing ^{12}C glucose. At indicated time points, cells were harvested and subjected to lipid extraction. The total lipid extract was analyzed with an UPLC-qTOF system.

The analytic inspection of the PC species in the mutant strain *gpt2* illustrates a similar lipid profile compared to wild type, with predominant PC 32:2 species followed by 34:2, 32:1 and 34:1 species (Figure 20). Hence, also no difference was detected in the remodeling kinetics in PC in the *gpt2* mutant (Figure 21).

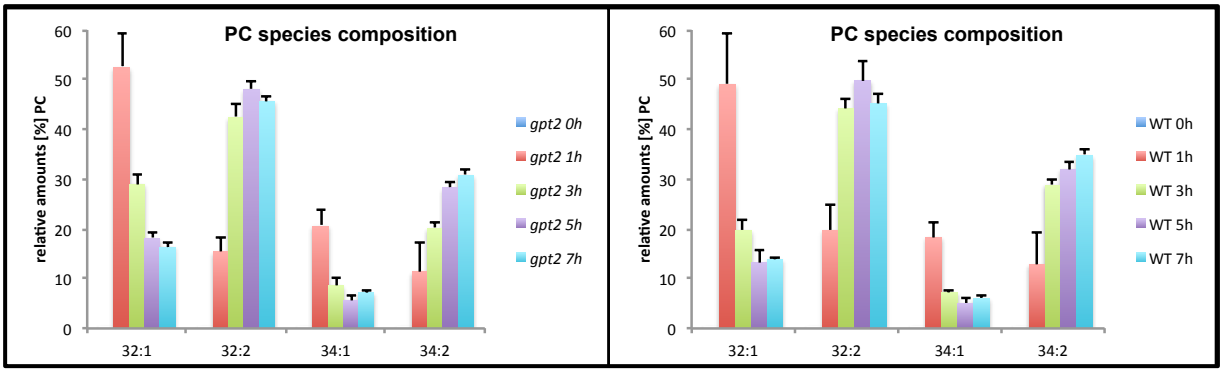

Figure 20: Relative amounts of PC lipid species in *gpt2* mutant compared to BY4742 WT cells at distinct time points.

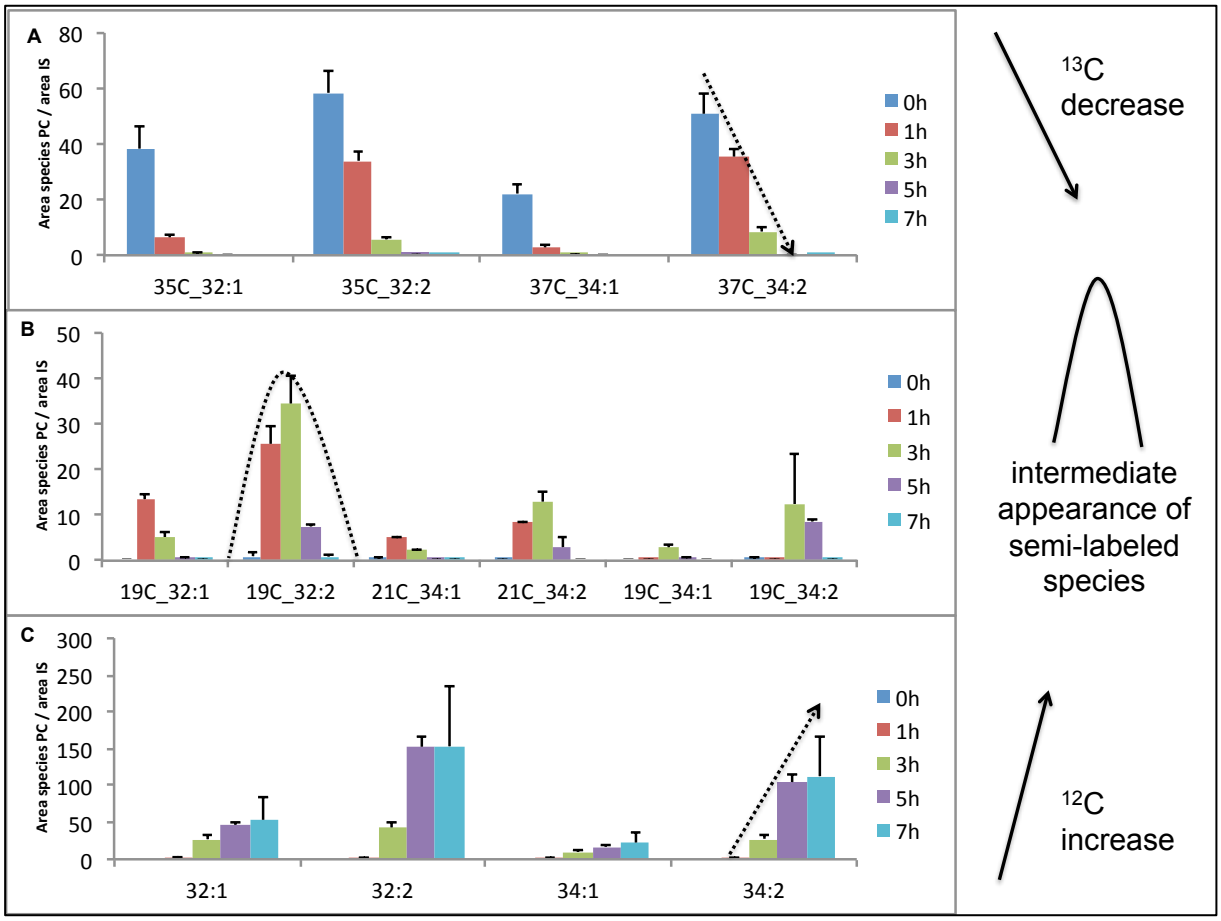

Figure 21: Detection of remodeling kinetics in phospholipids. (A) Decrease of fully labeled PC species. (B) Semi-labeled PC species. (C) Recovery of *de novo* synthesized PC species.

4.5 The contribution of the Kennedy pathway to phospholipid synthesis and turnover

Phosphatidylcholine (PC), the major phospholipid in yeast, can be built up via two different pathways, namely the CDP-DAG and the CDP-choline or Kennedy pathway (Kent, 1995). The cholinephosphate cytidylyltransferase Pct1 is a rate-determining enzyme of the CDP-choline pathway for phosphatidylcholine synthesis. The deletion

mutant *pct1,* defective in this pathway, was used to study how the activity of the PE methylation pathway is affected, when the Kennedy pathway is blocked. As shown in Figure 22, labeled and control cells show a growth behavior comparable to wild type cells (Figure 11).

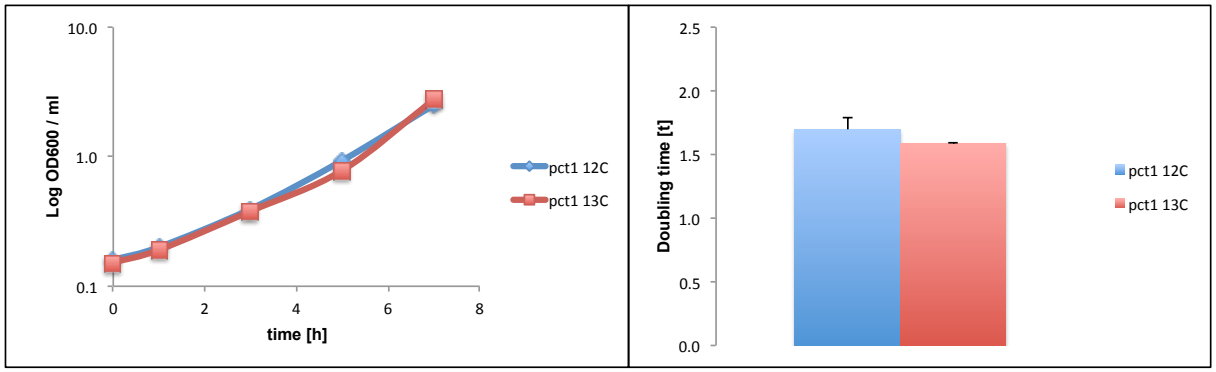

Figure 22: Growth curves and doubling times of the *pct1* mutant under ^{13}C and ^{12}C glucose conditions show comparable growth behavior.

Lipid extracts of the control cells and labeled cells were analyzed by ESI-MS to obtain lipid profiles of PE, PC, PI, DAG and TAG (Figure 23). The observation revealed that the profiles of *pct1* are similar to wild type lipid profiles shown in Figure 12 and neither the analytical investigation of PE and PC lipid species, nor the detection of remodeling kinetics illustrates significant differences to the wild type (Figure 25, Figure 26). The only difference in *de novo* synthesized lipid species between *pct1* cells compared to wild type was a significant accumulation of DAG (Figure 24). Overall, the Kennedy pathway does not appear to contribute significantly to net PC synthesis and remodeling under the experimental conditions.

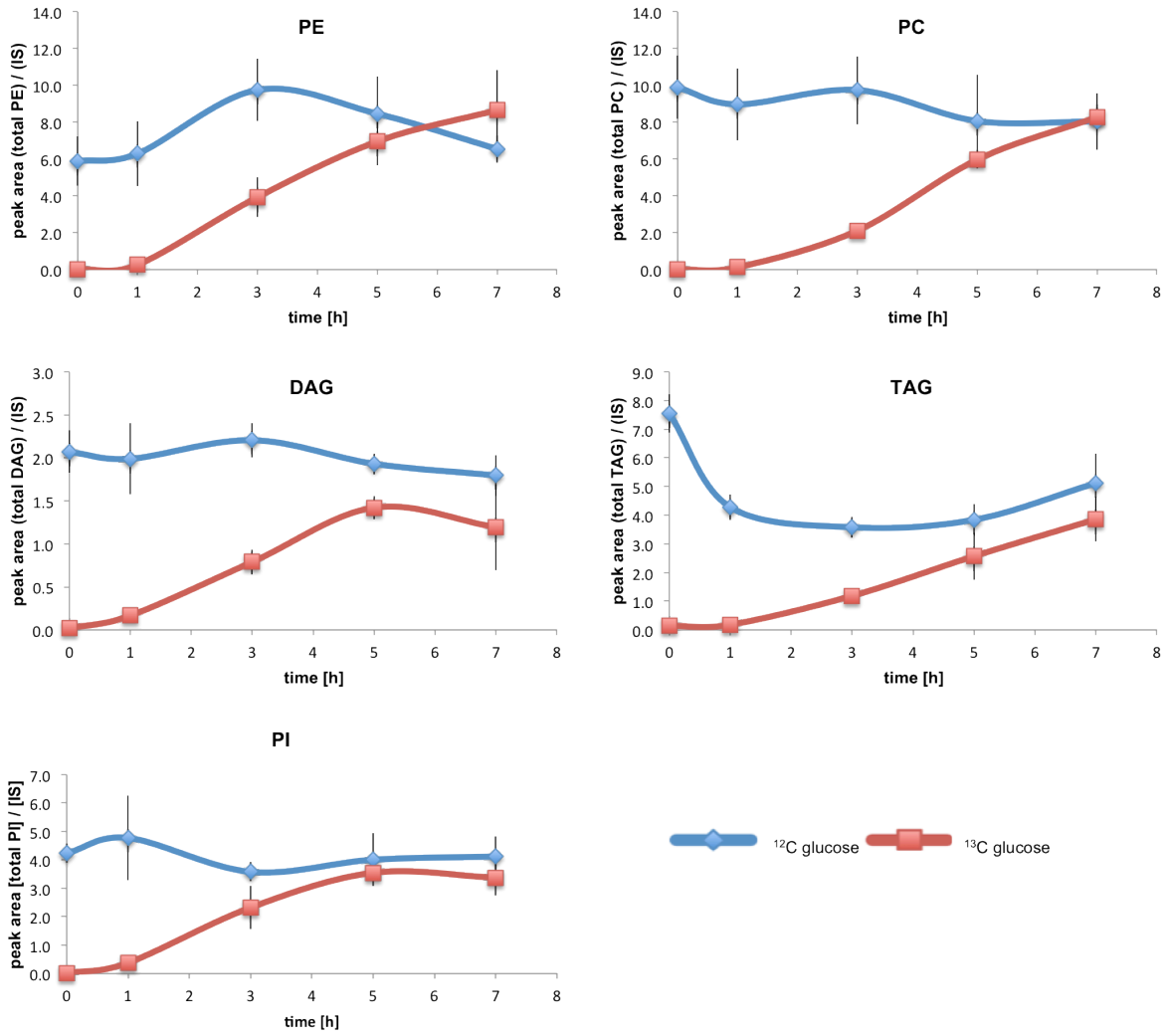

Figure 23: Lipid profile of *pct1* shows PE, PC, PI, DAG and TAG species. Cells were grown to late-logarithmic phase for 16 hours (time point zero) in medium with ^{13}C glucose and shifted to fresh medium containing ^{12}C glucose. Control cells were pre-cultivated in medium containing ^{12}C glucose and shifted to fresh medium containing ^{12}C glucose. At indicated time points (0, 1, 3, 5 and 7 hours) cells were harvested and subjected to lipid extraction. The total lipid extract was analyzed with a UPLC-qTOF system as described above.

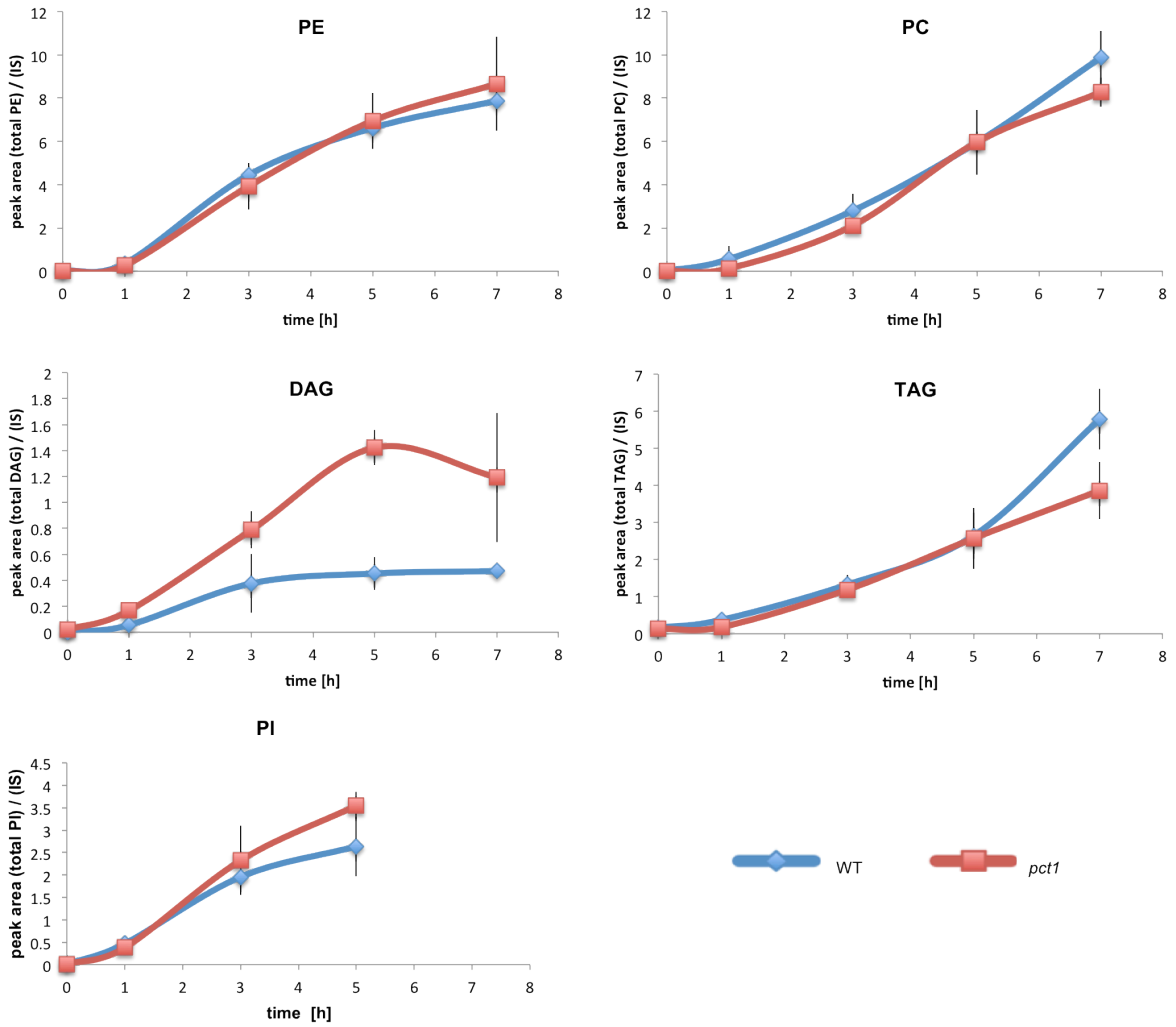

Figure 24: Lipid profile of the *pct1* mutant compared to wild type shows PE, PC, PI, DAG and TAG species. Cells were grown to late-logarithmic phase for 16 hours (time zero) in medium with 13C glucose and shifted to fresh medium containing ^{12}C glucose. At indicated time points, cells were harvested and subjected to lipid extraction. The total lipid extract was analyzed with an UPLC-qTOF system.

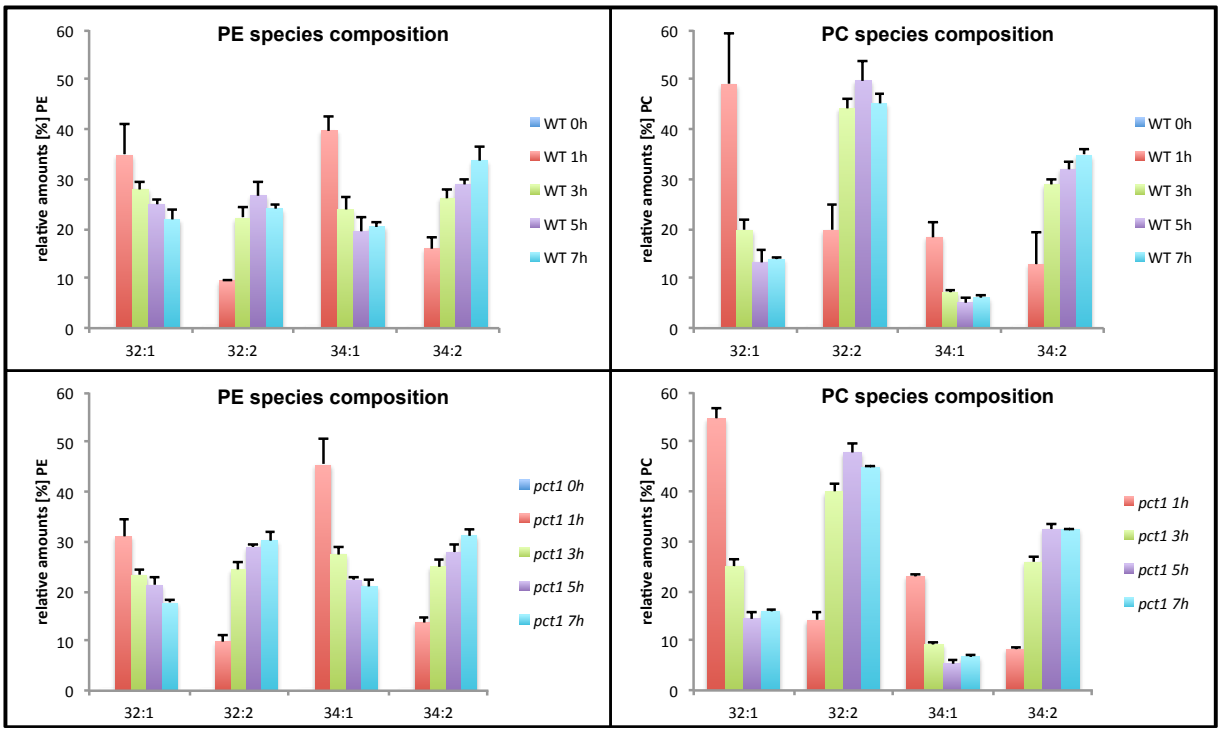

Figure 25: Relative amounts of PE and PC lipid species in the *pct1* mutant compared to BY4742 WT cells at distinct time points.

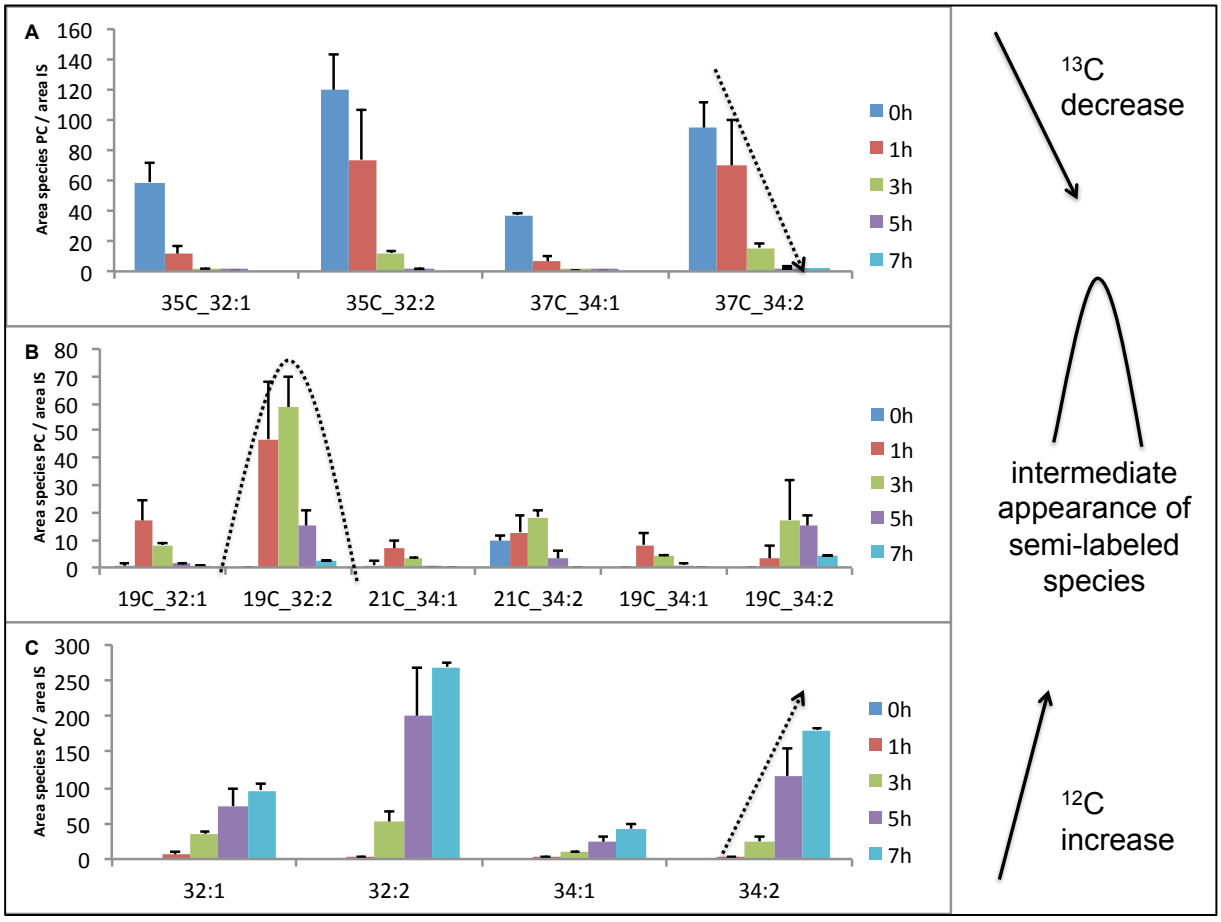

Figure 26: Detection of remodeling kinetics in phospholipids. (A) Decrease of fully labeled PC species. (B) Semi-labeled PC species. (C) Recovery of *de novo* synthesized PC species.

5 Summary

In conclusion, we established a new method for monitoring phospholipid and neutral lipid species in total lipid extracts. The method employs a specific "mass-tag" strategy by pre-cultivation of cells in ^{13}C glucose to produce labeled lipid species with carbon-specific mass offsets ("steady-state"). By shifting cells back to media containing ^{12}C glucose ("chase") recovery rates of lipid species are analyzed by mass spectrometry. The method is cheap, provides maximum labeling efficiency, comparable growth behavior of all analyzed strains and no major changes in cellular physiology. Moreover, media conditions are variable and, thus, suitable for supplementation studies, e.g. with unlabeled choline, ethanolamine, inositol and fatty acids (e.g. oleic acid). Analysis of wild type and several mutant strains showed an exchange of ^{13}C-carbon atoms in cellular lipids against ^{12}C-carbon atoms within 5 hours (PI) or 7 hours of growth (PE, PC, TAG and DAG) in unlabeled glucose. This rapid kinetics enabled the determination of *de novo* synthesis rates and also remodeling dynamics of lipid species. Moreover, we found that a mutant strain defective in the glycerol-3-phosphate acyltransferase Gpt2 showed a faster kinetics of DAG production and a reduced flux into PC and PE, compared to wild type, indicating a substantial contribution of Gpt2 to PL synthesis. In contrast, inhibition of the Kennedy pathway in the *pct1* mutant strain, lacking cholinephosphate cytidylyltransferase activity, did not lead to alterations in the phospholipid labeling kinetics. These data suggest that this pathway does not contribute significantly to net PC synthesis and remodeling in the absence of exogenous choline.

6 Discussion

Mass tag strategy to monitor *de novo* synthesized lipid species

In the last decade, numerous different approaches for the quantification of lipids have been established, by applying labeling techniques such as radiolabeling as well as stable isotope labeling (Balgoma et al., 2010; Borén et al., 2012). Thereby, *de novo* synthesized lipids can be distinguished from pre-existing pools. Additionally, flux lipidomics are applied to unravel information about synthesis, degradation as well as regulation of the lipid metabolism in time (Li et al., 2013). However, most of these techniques are established as pulse labeling experiments. We present here a new

stable isotopic labeling method combined with mass spectrometry (ESI-MS) to gain better insights into the lipid metabolism and its regulation. The method provides multiple benefits such as cost reduction due to pre-labeling of cells, whereby up to 90% of required labeling can be saved. Furthermore, the analyzed strains showed comparable growth behavior and doubling times. Additional advantages include variable media conditions for supplementation studies, e.g. with unlabeled choline, ethanolamine, inositol and fatty acids. Moreover, the method provides high labeling efficiency. However, 2 or 4 non-labeled carbon atoms could be detected in lipid species, which probably arise due to the supply of unlabeled amino acids to the growth media. We assume that amino acids are degraded to acetyl-CoA, which can be further used as a precursor for fatty acid biosynthesis. Extension of the labeling time did not lead to an increase in labeling efficiency either. The chosen experimental conditions in which cells are labeled to late-logarithmic growth phase to gain high labeling rates but still preventing cells from entering stationary phase and keeping them growing logarithmically even after the shift to media with ^{12}C glucose. However, a slight lag phase was still detected after shift to fresh media.
Noticeable is the observation that phospholipid head groups remained unlabeled in ^{13}C glucose containing media, also due to the proposed unlabeled amino acids supply. Choline and ethanolamine can be synthesized from methionine and serine. In the absence of precursors, the Kennedy pathway is active to recycle choline from lipid turnover (McMaster and Bell, 1994b). Thus, we would suggest conducting further studies with yeast strains that are prototrophic for amino acids (e.g. CEN.PK) to obtain complete carbon labeling.

In vivo kinetics in lipid metabolism of wild type yeast

Traditional methods in lipidomics only yield static estimations of lipid composition and hence limited mechanistic information, whereas kinetic studies enable further understanding of regulation, turnover and synthesis of lipids *in vivo* (Borén et al., 2012). Kinetics measurements of phospholipid acylation in wild type showed a full exchange of ^{13}C carbon atoms with ^{12}C carbon atoms within 5 hours in PI or 7 hours in TAG, indicating a fast turnover. Noticeable is also the observation that the phospholipid acylchain composition changes over time from mono- to di-unsaturated species, indicating that saturated and probably shorter fatty acids are synthesized and incorporated faster into lipid species in the first hours but are

exchanged afterwards against unsaturated and longer fatty acids. Furthermore, we showed that the species profile of PE differs from the PC profile: whereas the steady state profile of PE is dominated by PE 34:2, PC is enriched in 32:2 species. These results are in agreement with Boumann et al. 2004, indicating species selectivity of enzymes converting 32:2 PE into PC and/or acyl chain remodeling by phospholipase B activities (Boumann et al., 2004; De Smet et al., 2013).

Remodeling kinetics in phospholipids

Acyl-chain remodeling of phospholipids is required to maintain membrane lipid composition. Stable isotope labeling in combination with mass spectrometry allows monitoring of acyl chain remodeling, as exemplified for PC.

We demonstrate that an existing labeled fatty acid is replaced by an unlabeled *de novo* synthesized fatty acid. Semi-labeled fatty acids were never observed under these cultivation conditions, suggesting absence of fatty acid breakdown by β-oxidation. The predominant PC species in yeast are PC 32:2 and 34:2 and thus, the highest turnover was detected for this species. Furthermore, PC kinetics was rather constant over time as compared to PE. We conclude that remodeling plays an important role to sustain lipid homeostasis and membrane integrity. Taken together, these results confirm that the method is valuable to study remodeling kinetics *in vivo* and has great potential also for applications in higher eukaryotes.

The contribution of Gpt2 to phospholipid synthesis

To study the contribution of acyltransferases to phospholipid synthesis and turnover, we compared the lipid profiles from *gpt2* mutants and wild type cells. We noticed that a mutant strain defective in the glycerol-3-phosphate acyltransferase Gpt2 showed faster kinetics of DAG acylation and a reduced flux into PC and PE, compared to wild type, indicating a substantial contribution of Gpt2 to PL synthesis. We suggest that *gpt2* cells generate a different PA species composition, whereby DAG cannot be converted to PL via the Kennedy pathway and, hence, accumulate. TAG levels did not increase, because TAG accumulation may be dependent on active Gpt2 (Marr et al., 2012). We suggest studies using exogenous ^{12}C fatty acid supply to actively modulate and imbalance the cellular fatty acid profile to reveal more insights into substrate specificities of Gpt2 and consequences of *GPT2* deletion on the cellular lipid profile under excess fatty acid conditions.

The contribution of the Kennedy pathway to phospholipid synthesis and turnover

To gain insight into the possibility that the CDP-DAG pathway contributes differently to the molecular species distribution, lipid profiles of wild type cells were compared with those of *pct1* mutants lacking the CDP-choline route.

Investigations of the species profiles or remodeling kinetics did not reveal major alterations in the lipid composition between the *pct1* mutant and wild type cells. The only difference in *de novo* synthesized lipid species in *pct1* cells compared to wild type was a significant accumulation of DAG. As described in the literature, mutants lacking a functional CDP–choline pathway increase the rate of phospholipid synthesis via the CDP–DAG route to balance the lipid composition (Choi et al., 2004; Griac et al., 1996), which might explain the unchanged PL levels but the increased DAG pool. Interestingly, no differences in the lipid species composition were observed in the *pct1* mutant, indicating that both, Kennedy and CDP-DAG pathways are capable of generating the same species to sustain lipid homeostasis in the absence of exogenous choline supply. However, further studies have to be performed using choline, ethanolamine or fatty acid supply to reveal the exact mechanisms controlling PE and PC synthesis and remodeling.

7 Materials and Methods

7.1 Instrumentation

Table 1: Used instruments and software

Instruments	Company
Acquity UPLC® system	Waters
Autoclave	Systec
Bi-distillery	GFL®
Centrifuge 5810	Eppendorf
L-6200 gradient pump	Hitachi
Multi reax shaker	Heidolph
Synapt® G1 mass spectrometer	Waters
Trace gas chromatograph / flame ionization detector	Thermo Scientific
Trace GC Ultra gas chromatograph / DSQ mass spectrometer	Thermo Scientific
Columns	
BEH C18 1.7µm, 2.1x150mm	Waters
Betasil Diol-100 column 4.6x150 mm, 5 µm	Thermo Scientific
Software	Firma
Lipid Data Analyzer	Hartler et al. (2011)
Xcalibur 2.0	Thermo Scientific
MassLynx 4.1™	Waters

7.2 List of chemicals

Table 2: Used chemicals

Chemicals	Company
Acetone	Roth
Acetonitrile	J.T. Baker
Adenine	Sigma Aldrich
Ammonium acetate	Fluka
Ammonium persulfate	Bio-Rad
Ammonium sulfate	Roth
Arginine	Merck
Aspartic acid	Merck
Benzoic acid	Sigma Aldrich
Biotin	Merck
Boric acid	Merck

Boron triflouride	Sigma Aldrich
Calcium chloride	Fluka
Calicum pantothenate	Acros Organics
Chloroform	Sigma Aldrich
Copper sulfate	Merck
Folic acid	Sigma Aldrich
Formic acid	Merck
Glass beads	Sartorius
Glucose monohydrate	Roth
Glutamic acid	Sigma Aldrich
Glycine	AppliChem
Histidine monohydrochloride	Merck
Inositol	Aldrich
Iron chloride	Merck
Isooctane	Roth
Isopropanol	Roth
Leucine	Sigma Aldrich
Lysine monohydrochloride	Merck
Magnesium chloride	Merck
Magnesium sulphate	Roth
MES hydrate	Sigma Aldrich
Methanol	J.T. Bake
Methionine	Merck
Myristic acid	Fluka
n-Hexane	Roth
N,O-bis-trimethylsilyl-trifluoro-acetamide	Fluka
Niacin	Fluka
p-Aminobenzoic acid	Sigma Aldrich
Peptone	BD
Phenylalanine	Sigma Aldrich
Potassium dihydrogen phosphate	Roth
Pyridoxal hydrochloride	Calbiochem
Riboflavin	Sigma Aldrich
Serine	Sigma Aldrich
Sodium chloride	Roth
Sodium hydroxide	Merck
Thiamine hydrochloride	Sigma Aldrich
Threonine	Merck
Tris	Roth
Tryptophan	Merck
Tyrosin	Merck
Uracil	Sigma Aldrich
Valine	Sigma Aldrich
Water	in-house distillery
Whatman filters	GE Healthcare
Yeast extract	BD
Zinc sulfate	Roth

7.3 Cell cultivation

7.3.1 Strains used in this study

The following strains listed in table 3 have been used in this work.

Table 3: List of strains used in this work

Strain	Mat	Genotype	Source
BY4742 (WT)	α	*his3Δ1 leu2Δ0 lys2Δ0 ura3Δ0*	EUROSCARF
pct1	α	*YGR202C::KanMX4 his3Δ1 leu2Δ0 lys2Δ0 ura3Δ0*	EUROSCARF
gpt2	α	*YKR067W::kanMX4 his3Δ1 leu2Δ0 lys2Δ0 ura3Δ0*	EUROSCARF

7.3.2 Media conditions

The following part shows the composition of the utilized solutions and stock solutions (Table 4). All media have been autoclaved 20 minutes at 121°C and after cooling, heat instable reagents such as amino acids, vitamins and trace elements were added. These solutions were sterilized by sterile filtration. Plates for cell cultivation contained 20g/l of agar.

Table 4: Composition of used media

Minimal medium composition		
Amino acid and adenine stock solution (50x)	20	ml/l
Glucose monohydrate	22	g/l
Inositol stock solution (1000x)	1	ml/l
MES buffer 1(M pH6 with NaOH)	20	ml/l
Trace element stock solution (1000x)	1	ml/l
Uracil stock solution (500mg/250ml)	20	ml/l
Vitamin stock solution (400x)	2.5	ml/l
Yeast nitrogen base	6.7	g/l

Table 5: Composition of amino acid stock solution (Hanscho et al. (2012)), vitamin stock solution and trace element stock solution (Villa-Garcia et. al. (2011)), YNB and MES buffer

Uracil stock solution (50x)		
Uracil	2	g/l
Amino acid and adenine stock solution (50x)		
Adenine	2	g/l
Arginine	0.96	g/l
Aspartic acid	4.8	g/l
Glutamic acid	4.8	g/l
Histidine mono hydrochloride	2.28	g/l
Leucine	5.4	g/l
Lysine	7.2	g/l
Methionine	5.76	g/l
Phenylalanine	2.4	g/l
Serine	18	g/l
Threonine	9.6	g/l
Tryptophan	1.92	g/l
Tyrosine	0.72	g/l
Valine	7.2	g/l
Vitamine stock solution (400x)		
Biotin	0.8	mg/l
Calcium pantothenate	160	mg/l
Folic acid	0.8	mg/l
Niacin	160	mg/l
p-Aminobenzoic acid	80	mg/l
Pyridoxal hydrochloride	160	mg/l
Riboflavin	80	mg/l
Thiamine hydrochloride	160	mg/l
Trace element stock solution (1000x)		
Boric acid	500	mg/l
Copper sulfate * 5 H_2O	40	mg/l
Iron chloride + 6 H_2O	500	mg/l
Manganese sulfate * 7 H_2O	400	mg/l
Potassium iodate	100	mg/l
Sodium molybdate	200	mg/l
Zinc sufate * 7 H_2O	400	mg/l
Yeast nitrogen base		
Potassium dihydrogenphosphate	13.70	g
Magnesium sulfate * 7 H_2O	14.01	g
Sodium chloride	1.37	g
Calcium chloride * 2 H_2O	1.81	g
Ammonium sulfate * 7 H_2O	68.70	g
MES buffer (1M, pH 6 with NaOH)	195.2	g/l
Inositol stock solution (1000x)	13.5	g/l

7.3.3 Culture conditions

Cells were grown for 24 hours in defined minimal medium containing 75 µM inositol and ^{12}C glucose (Table 4), rediluted to $1 \cdot 10^5$ cells/ml in fresh minimal medium with ^{13}C glucose and grown for 16 hours to late logarithmic growth phase. The cells were then shifted to the main culture via filtration through a sterile 0.45 µm filter at an initial cell density of $1.2 \cdot 10^8$ cells/ml. The main culture medium contains minimal medium with ^{12}C glucose. $1.2 \cdot 10^8$ cells were harvested (3000 rpm, 4°C, 5 minutes) at time point 0, after 1 hour, 3 hours, 5 hours and 7 hours growth in ^{12}C glucose. Cell pellets were stored at -20°C until processing.

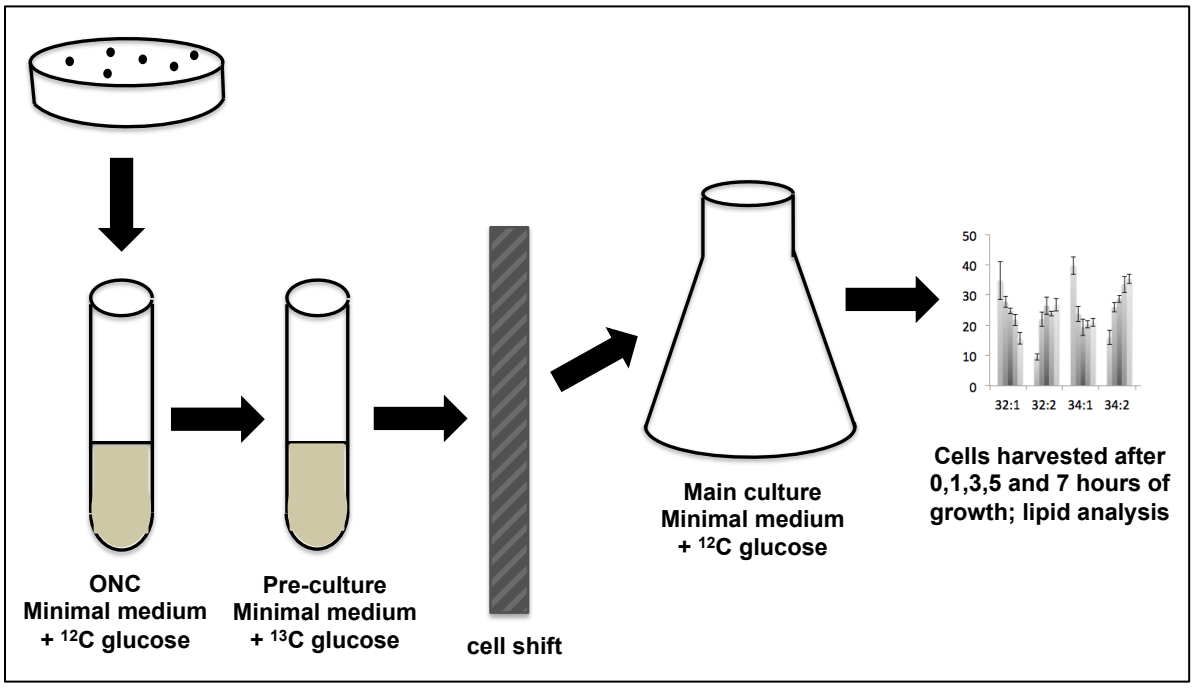

Figure 27: Experimental approach

7.4 Lipid analysis

7.4.1 Total lipid extraction

For total lipid extraction, cell pellets with 10 OD_{600} units of cells (equals $1.2 \cdot 10^8$ cells), were disrupted with 1ml glass beads in 5ml chloroform/methanol 2/1 (C/M 2/1) and 50 µl 0.05 mg/ml internal standard (table 7) in a 25ml Pyrex tube by shaking in a test tube shaker (Schwabach, Germany) for 30 minutes (level 10, 4°C). After 1ml of 0.0034% $MgCl_2$ was added, the sample was additionally shaken (10 minutes, 4°C). After centrifugation in a tabletop centrifuge for 3 minutes (3000 rpm, 4°C), the

aqueous upper phase was discarded with a glass Pasteur pipette and 2ml of an artificial upper phase methanol/water/chloroform (48/47/3, v/v/v) were added and carefully vortexed. After another centrifugation step, the aqueous upper phase was again discarded and the organic lower phase was transferred to a 15ml Pyrex tube. After that, the organic solvent was evaporated under N_2 stream and the lipids were dissolved in 1ml C/M 2/1 and stored in a micro vial at -20°C.

7.4.2 UPLC-qTOF analysis

For UPLC-qTOF measurement, the sample was diluted 1/5 with isopropanol (positive mode) or an aliquot was evaporated and dissolved 1/2 in 90% isopropanol 10% chloroform (negative mode). Lipid analysis was performed with an AQUITY-UPLC system (Waters Inc.) with a BEH-C18 (2.1 x 150 mm, 1.7 µm) column. For the positive mode the injection volume amounts to 5 µl, for the negative mode 10 µl. The chromatographic separation was performed with a binary gradient consisting of solvent A (water/methanol 1/1, v/v) and solvent B (isopropanol). Both solvents contained 10mM ammonium acetate, 0.1% formic acid and 8µM phosphoric acid. The settings of the linear gradient are described in table 6. The analysis was conducted with a flow rate of 150 µl/min and a source temperature of 100°C. The capillary voltage was set to 2.6 kV in positive mode and to 2.1 kV in negative mode. Leucine enkephalin (100 pg/µl in acetonitrile/water 1/1 with 0.1% formic acid) served as a reference and was injected into the MS system by a second HPLC pump (L-6200 gradient pump, Hitachi) at a flow rate of 150 µl/min splitted in a ratio 1/13. The internal standard was used for normalization of the data. The obtained data was evaluated with the software Lipid Data Analyzer (Hartler et al. 2011).

Table 6: UPLC - gradient

time [min]	solvent A [%]	solvent B [%]
0	55	45
30	10	90
32	0	100
42	0	100
43	55	45
50	55	45

Table 7: Internal standard composition

Lipid class	Acyl chain
PA	12:0/12:0
	14:0/14:0
	17:0/17:0
PS	17:0/17:0
PE	12:0/12:0
	17:0/17:0
PC	12:0/12:0
	17:0/17:0
	19:0/19:0
DAG	14:0/14:0
TAG	12:0/12:0/12:0
	15:0/15:0/15:0
	17:0/17:0/17:0
	19:0/19:0/19:0

7.4.3 Analysis of fatty acid methyl esters by GC-FID

To obtain fatty acid methyl esters (FAME), 200 µl of total lipid extract and 10 µl of butylhydroxytoluene were transferred into a 15 ml Pyrex tube and were dried under a steam of nitrogen. Afterwards, 0.5 ml toluene and 3 ml 2% water/methanol were added and incubated for 1 hour at 100°C in the drying oven. After that, samples were cooled in an ice-bath and 1 ml ice-cold water and 2 ml hexane/chloroform (4/1, v/v) were added and mixed for 15 minutes. Then, samples were centrifuged in a tabletop centrifuge for 3 minutes, 3000 rpm at 4°C. Three different phases can be distinguished. The upper phase is transferred to a glass tube and dried under stream of nitrogen. Subsequently, 1 ml ice-cold water and 2 ml hexane/chloroform (4/1, v/v) were added to the lower phase, mixed for 15 minutes and centrifuged (2000 rpm, 5 minutes). The upper phase was removed and pooled with the first upper phase and dried under a stream of nitrogen. The FAMEs were dissolved in 500 µl hexane and the solvent was evaporated under N_2 stream. After resolving in 100 µl hexane, the solution was transferred into an autosampler vial.

The calibration stock solutions (C16:0, C16:1, C18:0, C18:0) were diluted and subjected to the same protocol. Samples were analyzed on a Trace GC gas chromatograph combined with a flame ionization detector (Thermo Scientific). The obtained data were analyzed with the software Xcalibur 2.0 (Thermo Scientific).

7.4.4 Analysis of trimethylsilyl ethers of α-D-glucose by GC-MS

To obtain trimethylsilyl ethers of α-D-glucose, the glucose solution was diluted in water to a final concentration of 0,165 mg/ml. 200 µl were transferred to an autosampler vial and dried in the speed vac. 100 µl of a mixture of N,O-bis(trimethylsilyl-trifluoro-acetamide (BSTFA) and pyridine (1/2, v/v) was added. After 30 minutes of incubation at room temperature, the solution was analyzed on a Trace GC Ultra gas chromatograph combined with a DSQ mass spectrometer (Thermo Scientific) working in electron impact ionization mode. The obtained fragments were assigned to their elemental composition according to DeJongh et al. 1969.

8 References

Athenstaedt, K., and Daum, G. (2000). 1-Acyldihydroxyacetone-phosphate reductase (Ayr1p) of the yeast Saccharomyces cerevisiae encoded by the open reading frame YIL124w is a major component of lipid particles. J. Biol. Chem. *275*, 235–240.

Balgoma, D., Montero, O., Balboa, M.A., and Balsinde, J. (2010). Lipidomic approaches to the study of phospholipase A2-regulated phospholipid fatty acid incorporation and remodeling. Biochimie *92*, 645–650.

Benghezal, M., Roubaty, C., Veepuri, V., Knudsen, J., and Conzelmann, A. (2007). SLC1 and SLC4 encode partially redundant acyl-coenzyme A 1-acylglycerol-3-phosphate O-acyltransferases of budding yeast. J. Biol. Chem. *282*, 30845–30855.

Van den Berg, M.A., de Jong-Gubbels, P., Kortland, C.J., van Dijken, J.P., Pronk, J.T., and Steensma, H.Y. (1996). The two acetyl-coenzyme A synthetases of Saccharomyces cerevisiae differ with respect to kinetic properties and transcriptional regulation. J. Biol. Chem. *271*, 28953–28959.

Black, P.N., and DiRusso, C.C. (2007). Yeast acyl-CoA synthetases at the crossroads of fatty acid metabolism and regulation. Biochim. Biophys. Acta - Mol. Cell Biol. Lipids *1771*, 286–298.

Bleijerveld, O.B., Brouwers, J.F.H.M., Vaandrager, A.B., Helms, J.B., and Houweling, M. (2007). The CDP-ethanolamine pathway and phosphatidylserine decarboxylation generate different phosphatidylethanolamine molecular species. J. Biol. Chem. *282*, 28362–28372.

Borén, J., Taskinen, M.-R., and Adiels, M. (2012). Kinetic studies to investigate lipoprotein metabolism. J. Intern. Med. *271*, 166–173.

Boulton, C.A., and Ratledge, C. (1981). Correlation of Lipid Accumulation in Yeasts with Possession of ATP: Citrate Lyase. Microbiology *127*, 169–176.

Boumann, H.A., Damen, M.J.A., Versluis, C., Heck, A.J.R., De Kruijff, B., and De Kroon, A.I.P.M. (2003). The two biosynthetic routes leading to phosphatidylcholine in yeast produce different sets of molecular species. Evidence for lipid remodeling. Biochemistry *42*, 3054–3059.

Boumann, H.A., Chin, P.T.K., Heck, A.J.R., De Kruijff, B., and De Kroon, A.I.P.M. (2004). The yeast phospholipid N-methyltransferases catalyzing the synthesis of phosphatidylcholine preferentially convert di-C16:1 substrates both in vivo and in vitro. J. Biol. Chem. *279*, 40314–40319.

Brindle, J.T., Antti, H., Holmes, E., Tranter, G., Nicholson, J.K., Bethell, H.W.L., Clarke, S., Schofield, P.M., McKilligin, E., Mosedale, D.E., et al. (2002). Rapid and noninvasive diagnosis of the presence and severity of coronary heart disease using 1H-NMR-based metabonomics. Nat. Med. *8*, 1439–1444.

Carman, G.M., and Han, G.-S. (2011). Regulation of phospholipid synthesis in the yeast Saccharomyces cerevisiae. Annu. Rev. Biochem. *80*, 859–883.

Carman, G.M., and Henry, S. a (2007). Special issue: Regulation of lipid metabolism in yeast. Biochim. Biophys. Acta *1771*, 239–240.

Chang, Y.F., and Carman, G.M. (2008). CTP synthetase and its role in phospholipid synthesis in the yeast Saccharomyces cerevisiae. Prog. Lipid Res. *47*, 333–339.

Chatterjee, M.T., Khalawan, S.A., and Curran, B.P. (2001). Subtle alterations in growth medium composition can dramatically alter the percentage of unsaturated fatty acids in the yeast Saccharomyces cerevisiae. Yeast *18*, 81–88.

Chen, Y., Siewers, V., and Nielsen, J. (2012). Profiling of cytosolic and peroxisomal acetyl-CoA metabolism in Saccharomyces cerevisiae. PLoS One *7*.

Choi, H.-S., Sreenivas, A., Han, G.-S., and Carman, G.M. (2004). Regulation of phospholipid synthesis in the yeast cki1Delta eki1Delta mutant defective in the Kennedy pathway. The Cho1-encoded phosphatidylserine synthase is regulated by mRNA stability. J. Biol. Chem. *279*, 12081–12087.

Clancey, C.J., Chang, S.C., and Dowhan, W. (1993). Cloning of a gene (PSD1) encoding phosphatidylserine decarboxylase from Saccharomyces cerevisiae by complementation of an Escherichia coli mutant. J. Biol. Chem. *268*, 24580–24590.

Cowart, L.A., and Obeid, L.M. (2007). Yeast sphingolipids: Recent developments in understanding biosynthesis, regulation, and function. Biochim. Biophys. Acta - Mol. Cell Biol. Lipids *1771*, 421–431.

DeJongh, D.C. (1969). Analysis of Trimethylsilyl Derivatives of Carbohydrates by Gas Chromatography and Mass Spectrometry. *1*, 1728–1740.

Ejsing, C.S., Sampaio, J.L., Surendranath, V., Duchoslav, E., Ekroos, K., Klemm, R.W., Simons, K., and Shevchenko, A. (2009). Global analysis of the yeast lipidome by quantitative shotgun mass spectrometry. Proc. Natl. Acad. Sci. U. S. A. *106*, 2136–2141.

Faergeman, N.J., DiRusso, C.C., Elberger, A., Knudsen, J., and Black, P.N. (1997). Disruption of the Saccharomyces cerevisiae homologue to the murine fatty acid transport protein impairs uptake and growth on long-chain fatty acids. J. Biol. Chem. *272*, 8531–8538.

Faergeman, N.J., Black, P.N., Zhao, X.D., Knudsen, J., and DiRusso, C.C. (2001). The Acyl-CoA synthetases encoded within FAA1 and FAA4 in Saccharomyces cerevisiae function as components of the fatty acid transport system linking import, activation, and intracellular Utilization. J. Biol. Chem. *276*, 37051–37059.

Flick, J.S., and Thorner, J. (1993). Genetic and biochemical characterization of a phosphatidylinositol-specific phospholipase C in Saccharomyces cerevisiae. Mol. Cell. Biol. *13*, 5861–5876.

Fuchs, B., Schiller, J., Wagner, U., Häntzschel, H., and Arnold, K. (2005). The phosphatidylcholine/lysophosphatidylcholine ratio in human plasma is an indicator of the severity of rheumatoid arthritis: investigations by 31P NMR and MALDI-TOF MS. Clin. Biochem. *38*, 925–933.

Fuchs, B., Süß, R., Teuber, K., Eibisch, M., and Schiller, J. (2011). Lipid analysis by thin-layer chromatography-A review of the current state. J. Chromatogr. A *1218*, 2754–2774.

Fujita, M., and Jigami, Y. (2008). Lipid remodeling of GPI-anchored proteins and its function. Biochim. Biophys. Acta - Gen. Subj. *1780*, 410–420.

Fujiwaki, T., Yamaguchi, S., Sukegawa, K., and Taketomi, T. (2002). Application of delayed extraction matrix-assisted laser desorption ionization time-of-flight mass spectrometry for analysis of sphingolipids in cultured skin fibroblasts from sphingolipidosis patients. Brain Dev *24*, 170–3.

Fuller, M., Sharp, P.C., Rozaklis, T., Whitfield, P.D., Blacklock, D., Hopwood, J.J., and Meikle, P.J. (2005). Urinary lipid profiling for the identification of fabry hemizygotes and heterozygotes. Clin. Chem. *51*, 688–694.

Galdieri, L., and Vancura, A. (2012). Acetyl-CoA Carboxylase Regulates Global Histone Acetylation. J. Biol. Chem. *287*, 23865–23876.

Goffeau, A., Barrell, B.G., Bussey, H., Davis, R.W., Dujon, B., Feldmann, H., Galibert, F., Hoheisel, J.D., Jacq, C., Johnston, M., et al. (1996). Life with 6000 genes. Science *274*, 546, 563–567.

Griac, P., Swede, M.J., and Henry, S.A. (1996). The role of phosphatidylcholine biosynthesis in the regulation of the INO1 gene of yeast. J. Biol. Chem. *271*, 25692–25698.

Guan, X.L., Souza, C.M., Pichler, H., Dewhurst, G., Schaad, O., Kajiwara, K., Wakabayashi, H., Ivanova, T., Castillon, G.A., Piccolis, M., et al. (2009). Functional interactions between sphingolipids and sterols in biological membranes regulating cell physiology. Mol. Biol. Cell *20*, 2083–2095.

Han, X., and Gross, R.W. (2003). Global analyses of cellular lipidomes directly from crude extracts of biological samples by ESI mass spectrometry: a bridge to lipidomics. J. Lipid Res. *44*, 1071–1079.

Han, G.-S., Wu, W.-I., and Carman, G.M. (2006). The Saccharomyces cerevisiae Lipin homolog is a Mg2+-dependent phosphatidate phosphatase enzyme. J. Biol. Chem. *281*, 9210–9218.

Han, G.-S., O'Hara, L., Siniossoglou, S., and Carman, G.M. (2008). Characterization of the yeast DGK1-encoded CTP-dependent diacylglycerol kinase. J. Biol. Chem. *283*, 20443–20453.

Han, S.-H., Han, G.-S., Iwanyshyn, W.M., and Carman, G.M. (2005). Regulation of the PIS1-encoded phosphatidylinositol synthase in Saccharomyces cerevisiae by zinc. J. Biol. Chem. *280*, 29017–29024.

Han, X., Yang, J., Yang, K., Zhao, Z., Abendschein, D.R., and Gross, R.W. (2007). Alterations in myocardial cardiolipin content and composition occur at the very earliest stages of diabetes: a shotgun lipidomics study. Biochemistry *46*, 6417–6428.

Hartler, J., Trötzmüller, M., Chitraju, C., Spener, F., Köfeler, H.C., and Thallinger, G.G. (2011). Lipid Data Analyzer: unattended identification and quantitation of lipids in LC-MS data. Bioinformatics *27*, 572–577.

Hasslacher, M., Ivessa, A.S., Paltauf, F., and Kohlwein, S.D. (1993). Acetyl-CoA carboxylase from yeast is an essential enzyme and is regulated by factors that control phospholipid metabolism. J. Biol. Chem. *268*, 10946–10952.

Henry, S. a, Kohlwein, S.D., and Carman, G.M. (2012). Metabolism and regulation of glycerolipids in the yeast Saccharomyces cerevisiae. Genetics *190*, 317–349.

Hjelmstad, R.H., and Bell, R.M. (1987). Mutants of Saccharomyces cerevisiae defective in sn-1,2-diacylglycerol cholinephosphotransferase. Isolation, characterization, and cloning of the CPT1 gene. J. Biol. Chem. *262*, 3909–3917.

Hjelmstad, R.H., and Bell, R.M. (1988). The sn-1,2-diacylglycerol ethanolaminephosphotransferase activity of Saccharomyces cerevisiae. Isolation of mutants and cloning of the EPT1 gene. J. Biol. Chem. *263*, 19748–19757.

Hjelmstad, R.H., and Bell, R.M. (1991). sn-1,2-diacylglycerol choline- and ethanolaminephosphotransferases in Saccharomyces cerevisiae. Nucleotide sequence of the EPT1 gene and comparison of the CPT1 and EPT1 gene products. J. Biol. Chem. *266*, 5094–5103.

Hosaka, K., Kodaki, T., and Yamashita, S. (1989). Cloning and characterization of the yeast CKI gene encoding choline kinase and its expression in Escherichia coli. J. Biol. Chem. *264*, 2053–2059.

Hu, C., van der Heijden, R., Wang, M., van der Greef, J., Hankemeier, T., and Xu, G. (2009). Analytical strategies in lipidomics and applications in disease biomarker discovery. J. Chromatogr. B Anal. Technol. Biomed. Life Sci. *877*, 2836–2846.

Hunte, C., and Richers, S. (2008). Lipids and membrane protein structures. Curr. Opin. Struct. Biol. *18*, 406–411.

Jia, L., Wang, C., Zhao, S., Lu, X., and Xu, G. (2007). Metabolomic identification of potential phospholipid biomarkers for chronic glomerulonephritis by using high performance liquid chromatography-mass spectrometry. J. Chromatogr. B Anal. Technol. Biomed. Life Sci. *860*, 134–140.

Katajamaa, M., and Oresic, M. (2007). Data processing for mass spectrometry-based metabolomics. J. Chromatogr. A *1158*, 318–328.

Kennedy, E.P., and Weiss, S.B. (1956). The function of cytidine coenzymes in the biosynthesis of phospholipides. J. Biol. Chem. *222*, 193–214.

Kent, C. (1995). Eukaryotic phospholipid biosynthesis. Annu. Rev. Biochem. *64*, 315–343.

Kersting, M.C., and Carman, G.M. (2006). Regulation of the Saccharomyces cerevisiae EKI1-encoded ethanolamine kinase by zinc depletion. J. Biol. Chem. *281*, 13110–13116.

Kim, K., Kim, K.H., Storey, M.K., Voelker, D.R., and Carman, G.M. (1999). Isolation and characterization of the Saccharomyces cerevisiae EKI1 gene encoding ethanolamine kinase. J. Biol. Chem. *274*, 14857–14866.

Klig, L.S., and Henry, S.A. (1984). Isolation of the yeast INO1 gene: located on an autonomously replicating plasmid, the gene is fully regulated. Proc. Natl. Acad. Sci. U. S. A. *81*, 3816–3820.

Klose, C., Surma, M.A., Gerl, M.J., Meyenhofer, F., Shevchenko, A., and Simons, K. (2012). Flexibility of a eukaryotic lipidome - insights from yeast lipidomics. PLoS One *7*.

Klug, L., and Daum, G. (2014). Yeast lipid metabolism at a glance. FEMS Yeast Res. 369–388.

Knittelfelder, O.L., Weberhofer, B.P., Eichmann, T.O., Kohlwein, S.D., and Rechberger, G.N. (2014). A versatile ultra-high performance LC-MS method for lipid profiling. J. Chromatogr. B Anal. Technol. Biomed. Life Sci. *951-952*, 119–128.

Kodaki, T., and Yamashita, S. (1987). Yeast phosphatidylethanolamine methylation pathway. Cloning and characterization of two distinct methyltransferase genes. J. Biol. Chem. *262*, 15428–15435.

Köfeler, H.C., Fauland, A., Rechberger, G.N., and Trötzmüller, M. (2012). Mass Spectrometry Based Lipidomics: An Overview of Technological Platforms. Metabolites *2*, 19–38.

Kohlwein, S.D. (2010a). Obese and anorexic yeasts: experimental models to understand the metabolic syndrome and lipotoxicity. Biochim. Biophys. Acta *1801*, 222–229.

Kohlwein, S.D. (2010b). Triacylglycerol homeostasis: insights from yeast. J. Biol. Chem. *285*, 15663–15667.

Kohlwein, S.D., and Petschnigg, J. (2007). SLipid-induced cell dysfunction and cell death: lessons from yeast. Curr. Hypertens. Rep. *9*, 455–461.

Kohlwein, S.D., Veenhuis, M., and van der Klei, I.J. (2013). Lipid droplets and peroxisomes: key players in cellular lipid homeostasis or a matter of fat--store ’em up or burn 'em down. Genetics *193*, 1–50.

De Kroon, A.I.P.M., Rijken, P.J., and De Smet, C.H. (2013). Checks and balances in membrane phospholipid class and acyl chain homeostasis, the yeast perspective. Prog. Lipid Res. *52*, 374–394.

Kurat, C.F., Natter, K., Petschnigg, J., Wolinski, H., Scheuringer, K., Scholz, H., Zimmermann, R., Leber, R., Zechner, R., and Kohlwein, S.D. (2006). Obese yeast: triglyceride lipolysis is functionally conserved from mammals to yeast. J. Biol. Chem. *281*, 491–500.

Letts, V.A., Klig, L.S., Bae-Lee, M., Carman, G.M., and Henry, S.A. (1983). Isolation of the yeast structural gene for the membrane-associated enzyme phosphatidylserine synthase. Proc. Natl. Acad. Sci. U. S. A. *80*, 7279–7283.

Li, J., Hoene, M., Zhao, X., Chen, S., Wei, H., Häring, H.-U., Lin, X., Zeng, Z., Weigert, C., Lehmann, R., et al. (2013). Stable isotope-assisted lipidomics combined with nontargeted isotopomer filtering, a tool to unravel the complex dynamics of lipid metabolism. Anal. Chem. *85*, 4651–4657.

Li, M., Zhou, Z., Nie, H., Bai, Y., and Liu, H. (2011). Recent advances of chromatography and mass spectrometry in lipidomics. Anal. Bioanal. Chem. *399*, 243–249.

Loewen, C.J.R., Gaspar, M.L., Jesch, S.A., Delon, C., Ktistakis, N.T., Henry, S.A., and Levine, T.P. (2004). Phospholipid metabolism regulated by a transcription factor sensing phosphatidic acid. Science *304*, 1644–1647.

Mangold, H.K. (1961). Thin-layer chromatography of lipids. J. Am. Oil Chem. Soc. *38*, 708–727.

Marr, N., Foglia, J., Terebiznik, M., Athenstaedt, K., and Zaremberg, V. (2012). Controlling Lipid Fluxes at Glycerol-3-phosphate Acyltransferase Step in Yeast: Unique contribution of Gat1p to oleic acid-induced lipid particle formation. J. Biol. Chem. *287*, 10251–10264.

McDonough, V.M., Buxeda, R.J., Bruno, M.E., Ozier-Kalogeropoulos, O., Adeline, M.T., McMaster, C.R., Bell, R.M., and Carman, G.M. (1995). Regulation of phospholipid biosynthesis in Saccharomyces cerevisiae by CTP. J. Biol. Chem. *270*, 18774–18780.

McGraw, P., and Henry, S.A. (1989). Mutations in the Saccharomyces cerevisiae opi3 gene: effects on phospholipid methylation, growth and cross-pathway regulation of inositol synthesis. Genetics *122*, 317–330.

McMaster, C.R., and Bell, R.M. (1994a). Phosphatidylcholine biosynthesis via the CDP-choline pathway in Saccharomyces cerevisiae. Multiple mechanisms of regulation. J. Biol. Chem. *269*, 14776–14783.

McMaster, C.R., and Bell, R.M. (1994b). Phosphatidylcholine biosynthesis in Saccharomyces cerevisiae. Regulatory insights from studies employing null and chimeric sn-1,2-diacylglycerol choline- and ethanolaminephosphotransferases. J. Biol. Chem. *269*, 28010–28016.

Merkel, O., Oskolkova, O. V, Raab, F., El-Toukhy, R., and Paltauf, F. (2005). Regulation of activity in vitro and in vivo of three phospholipases B from Saccharomyces cerevisiae. Biochem. J. *387*, 489–496.

Min-Seok, R., Kawamata, Y., Nakamura, H., Ohta, A., and Takagi, M. (1996). Isolation and characterization of ECT1 gene encoding CTP: phosphoethanolamine cytidylyltransferase of Saccharomyces cerevisiae. J. Biochem. *120*, 1040–1047.

Moonlenaar, W.H. (1997). Lysophosphatidic acid : G-protein signalling and cellular responses. Curr. Opin. Cell. Biochem. *9*, 168–173.

Murphy, S. a, and Nicolaou, A. (2013). Lipidomics applications in health, disease and nutrition research. Mol. Nutr. Food Res. *57*, 1336–1346.

Murray, M., and Greenberg, M.L. (2000). Expression of yeast INM1 encoding inositol monophosphatase is regulated by inositol, carbon source and growth stage and is decreased by lithium and valproate. Mol. Microbiol. *36*, 651–661.

Natter, K., and Kohlwein, S.D. (2012). Yeast and cancer cells – common principles in lipid metabolism. Biochim. Biophys. Acta - Mol. Cell Biol. Lipids.

Nelson, L. D., Cox, M. M. (2004). Lehninger - Prinziples of Biochemistry. W. H. Freeman. Fourth edition, 355-356.

Nikawa, J., and Yamashita, S. (1984). Molecular cloning of the gene encoding CDPdiacylglycerol-inositol 3-phosphatidyl transferase in Saccharomyces cerevisiae. Eur. J. Biochem. *143*, 251–256.

Nikawa, J., Tsukagoshi, Y., and Yamashita, S. (1991). Isolation and characterization of two distinct myo-inositol transporter genes of Saccharomyces cerevisiae. J. Biol. Chem. *266*, 11184–11191.

Oh, C.S., Toke, D.A., Mandala, S., and Martin, C.E. (1997). ELO2 and ELO3, homologues of the Saccharomyces cerevisiae ELO1 gene, function in fatty acid elongation and are required for sphingolipid formation. J. Biol. Chem. *272*, 17376–17384.

Patrick C Choy, Yaw L Siow, David Mymin, K.O. (2004). Lipids and atherosclerosis. Biochem. Cell Biol. *82*, 212–224.

Paulus, H., Kennedy, E.P., and Kennedy, P. (1960). The Enzymatic Synthesis of Inositol Monophosphatide. The Journal of Biological Chemistry. 235, 1304-1311.

Pietiläinen, K.H., Sysi-Aho, M., Rissanen, A., Seppänen-Laakso, T., Yki-Järvinen, H., Kaprio, J., and Oresic, M. (2007). Acquired obesity is associated with changes in the serum lipidomic profile independent of genetic effects-a monozygotic twin study. PLoS One *2*, e218.

Pulfer, M., and Murphy, R.C. (2003). Electrospray mass spectrometry of phospholipids. Mass Spectrom. Rev. *22*, 332–364.

Pynn, C.J., Henderson, N.G., Clark, H., Koster, G., Bernhard, W., and Postle, A.D. (2011). Specificity and rate of human and mouse liver and plasma phosphatidylcholine synthesis analyzed in vivo. J. Lipid Res. *52*, 399–407.

Rudge, S.A., Pettitt, T.R., Zhou, C., Wakelam, M.J., and Engebrecht, J.A. (2001). SPO14 separation-of-function mutations define unique roles for phospholipase D in secretion and cellular differentiation in Saccharomyces cerevisiae. Genetics *158*, 1431–1444.

Schlame, M., Rua, D., and Greenberg, M.L. (2000). The biosynthesis and functional role of cardiolipin. Prog. Lipid Res. *39*, 257–288.

Shen, H., Heacock, P.N., Clancey, C.J., and Dowhan, W. (1996). The CDS1 gene encoding CDP-diacylglycerol synthase in Saccharomyces cerevisiae is essential for cell growth. J. Biol. Chem. *271*, 789–795.

Shindou, H., Hishikawa, D., Harayama, T., Yuki, K., and Shimizu, T. (2009). Recent progress on acyl CoA: lysophospholipid acyltransferase research. J. Lipid Res. *50 Suppl*, 46–51.

De Smet, C.H., Vittone, E., Scherer, M., Houweling, M., Liebisch, G., Brouwers, J.F., and de Kroon, A.I.P.M. (2012). The yeast acyltransferase Sct1p regulates fatty acid desaturation by competing with the desaturase Ole1p. Mol. Biol. Cell *23*, 1146–1156.

De Smet, C.H., Cox, R., Brouwers, J.F., and de Kroon, A.I.P.M. (2013). Yeast cells accumulate excess endogenous palmitate in phosphatidylcholine by acyl chain remodeling involving the phospholipase B Plb1p. Biochim. Biophys. Acta *1831*, 1167–1176.

Smith, R.D., Loo, J.A., Edmonds, C.G., Barinaga, C.J., and Udseth, H.R. (1990). New developments in biochemical mass spectrometry: electrospray ionization. Anal. Chem. *62*, 882–899.

Soto, A., and Carman, G.M. (2008). Regulation of the Saccharomyces cerevisiae CKI1-encoded choline kinase by zinc depletion. J. Biol. Chem. *283*, 10079–10088.

Stukey, J.E., McDonough, V.M., and Martin, C.E. (1990). The OLE1 gene of Saccharomyces cerevisiae encodes the delta 9 fatty acid desaturase and can be functionally replaced by the rat stearoyl-CoA desaturase gene. J. Biol. Chem. *265*, 20144–20149.

Summers, E.F., Letts, V.A., McGraw, P., and Henry, S.A. (1988). Saccharomyces cerevisiae cho2 mutants are deficient in phospholipid methylation and cross-pathway regulation of inositol synthesis. Genetics *120*, 909–922.

Sweeley, C.C., Bentley, R., Ma, M., and Gas-liquid, W.W.W. (1963). Gas-liquid chromatography of trimethylsilyl derivatives of sugars and related substances. J. Am. Chem. Soc. *85:2497-50*.

Takahashi, H., McCaffery, J.M., Irizarry, R.A., and Boeke, J.D. (2006). Nucleocytosolic Acetyl-Coenzyme A Synthetase Is Required for Histone Acetylation and Global Transcription. Mol. Cell *23*, 207–217.

Tehlivets, O., Hasslacher, M., and Kohlwein, S.D. (2004). S-Adenosyl-L-homocysteine hydrolase in yeast: Key enzyme of methylation metabolism and coordinated regulation with phospholipid synthesis. FEBS Lett. *577*, 501–506.

Tehlivets, O., Scheuringer, K., and Kohlwein, S.D. (2007). Fatty acid synthesis and elongation in yeast. Biochim. Biophys. Acta - Mol. Cell Biol. Lipids *1771*, 255–270.

Thevelein, J.M. (1994). Signal transduction in yeast. Yeast *10*, 1753–1790.

Touchstone, J.C. (1995). Thin-layer chromatographic procedures for lipid separation. J. Chromatogr. B Biomed. Appl. *671*, 169–195.

Trotter, P.J., Pedretti, J., and Voelker, D.R. (1993). Phosphatidylserine decarboxylase from Saccharomyces cerevisiae. Isolation of mutants, cloning of the gene, and creation of a null allele. J. Biol. Chem. *268*, 21416–21424.

Trotter, P.J., Pedretti, J., Yates, R., and Voelker, D.R. (1995). Phosphatidylserine decarboxylase 2 of Saccharomyces cerevisiáe. Cloning and mapping of the gene, heterologous expression, and creation of the null allele. J. Biol. Chem. *270*, 6071–6080.

Tsukagoshi, Y., Nikawa, J., and Yamashita, S. (1987). Molecular cloning and characterization of the gene encoding cholinephosphate cytidylyltransferase in Saccharomyces cerevisiae. Eur. J. Biochem. *169*, 477–486.

Tuller, G., Nemec, T., Hrastnik, C., and Daum, G. (1999). Lipid composition of subcellular membranes of an FY1679-derived haploid yeast wild-type strain grown on different carbon sources. Yeast *15*, 1555–1564.

Valianpour, F., Wanders, R.J.A., Barth, P.G., Overmars, H., and van Gennip, A.H. (2002). Quantitative and compositional study of cardiolipin in platelets by electrospray ionization mass spectrometry: application for the identification of Barth syndrome patients. Clin. Chem. *48*, 1390–1397.

Vihervaara, T., Suoniemi, M., and Laaksonen, R. (2013). Lipidomics in drug discovery. Drug Discov. Today.

Wagner, S., and Paltauf, F. (1994). Generation of glycerophospholipid molecular species in the yeast Saccharomyces cerevisiae. Fatty acid pattern of phospholipid classes and selective acyl turnover at sn-1 and sn-2 positions. Yeast *10*, 1429–1437.

Wang, C., Kong, H., Guan, Y., Yang, J., Gu, J., Yang, S., and Xu, G. (2005). Plasma phospholipid metabolic profiling and biomarkers of type 2 diabetes mellitus based on high-performance liquid chromatography/electrospray mass spectrometry and multivariate statistical analysis. Anal. Chem. *77*, 4108–4116.

Watson, A.D. (2006). Thematic review series: systems biology approaches to metabolic and cardiovascular disorders. Lipidomics: a global approach to lipid analysis in biological systems. J. Lipid Res. *47*, 2101–2111.

Wellen, K.E., Hatzivassiliou, G., Sachdeva, U.M., Bui, T. V, Cross, J.R., and Thompson, C.B. (2009). ATP-citrate lyase links cellular metabolism to histone acetylation. Science *324*, 1076–1080.

Wenk, M.R. (2010). Lipidomics: New tools and applications. Cell *143*, 888–895.

Wu, W.I., and Carman, G.M. (1996). Regulation of phosphatidate phosphatase activity from the yeast Saccharomyces cerevisiae by phospholipids. Biochemistry *35*, 3790–3796.

Xiao, Y.J., Schwartz, B., Washington, M., Kennedy, A., Webster, K., Belinson, J., and Xu, Y. (2001). Electrospray ionization mass spectrometry analysis of lysophospholipids in human ascitic fluids: comparison of the lysophospholipid contents in malignant vs nonmalignant ascitic fluids. Anal. Biochem. *290*, 302–313.

Yamashita, A., Sugiura, T., and Waku, K. (1997). Acyltransferases and transacylases involved in fatty acid remodeling of phospholipids and metabolism of bioactive lipids in mammalian cells. J. Biochem. *122*, 1–16.

Zaccheo, O., Dinsdale, D., Meacock, P.A., and Glynn, P. (2004). Neuropathy target esterase and its yeast homologue degrade phosphatidylcholine to glycerophosphocholine in living cells. J. Biol. Chem. *279*, 24024–24033.

Zaremberg, V., and McMaster, C.R. (2002). Differential partitioning of lipids metabolized by separate yeast glycerol-3-phosphate acyltransferases reveals that phospholipase D generation of phosphatidic acid mediates sensitivity to choline-containing lysolipids and drugs. J. Biol. Chem. *277*, 39035–39044.

Zheng, Z., and Zou, J. (2001). The initial step of the glycerolipid pathway: identification of glycerol 3-phosphate/dihydroxyacetone phosphate dual substrate acyltransferases in Saccharomyces cerevisiae. J. Biol. Chem. *276*, 41710–41716.

9 Appendix

9.1 GC-FID analysis

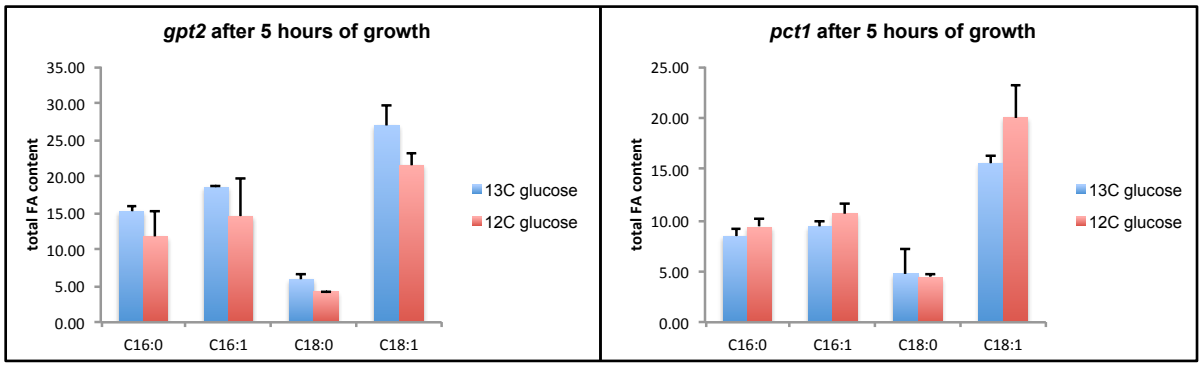

Figure 28: GC-FID analysis of labeled and unlabeled *gpt2* and *pct1* cells at 5 hours of growth displays comparable FA compositions.

9.2 Mass lists for LDA

Table 8: PE mass list

Side chain	dbs	C	H	O	P	N	D	M	[M+H]+	$[M+H]^+$	**$[M+Na]^+$**	tR (min)
28 :	0	33	66	8	1	1	0	635.452564	636.460389	**636.460389**	**658.442364**	14.45
28 :	1	33	64	8	1	1	0	633.436913	634.444739	**634.444739**	**656.426713**	12.67
30 :	0	35	70	8	1	1	0	663.483864	664.491689	**664.491689**	**686.473664**	16.58
30 :	1	35	68	8	1	1	0	661.468214	662.476039	**662.476039**	**684.458014**	14.89
30 :	2	35	66	8	1	1	0	659.452564	660.460389	**660.460389**	**682.442364**	13.22
32 :	1	37	72	8	1	1	0	689.499514	690.507339	**690.507339**	**712.489314**	16.95
32 :	2	37	70	8	1	1	0	687.483864	688.491689	**688.491689**	**710.473664**	15.28
34 :	1	39	76	8	1	1	0	717.530814	718.538639	**718.538639**	**740.520614**	18.91
34 :	2	39	74	8	1	1	0	715.515164	716.522989	**716.522989**	**738.504964**	17.32
36 :	1	41	80	8	1	1	0	745.562114	746.569939	**746.569939**	**768.551914**	20.68
36 :	2	41	78	8	1	1	0	743.546464	744.554289	**744.554289**	**766.536264**	19.24
IS24 :	0	29	58	8	1	1	0	579.389963	580.397788	**580.397788**	**602.379763**	9.86
IS34 :	0	39	78	8	1	1	0	719.546464	720.554289	**720.554289**	**742.536264**	20.44

Table 9: PC mass list

Side chain	dbs	C	H	O	P	N	D	M	[M+H]$^+$	[M+H]$^+$	**[M+Na]$^+$**	tR (min)
28 :	0	36	72	8	1	1	0	677.499514	678.507339	**678.5073386**	**700.4893**	13.99
28 :	1	36	70	8	1	1	0	675.483864	676.491689	**676.4916886**	**698.4737**	12.23
30 :	0	38	76	8	1	1	0	705.530814	706.538639	**706.5386387**	**728.5206**	16.18
30 :	1	38	74	8	1	1	0	703.515164	704.522989	**704.5229887**	**726.5050**	14.45
30 :	2	38	72	8	1	1	0	701.499514	702.507339	**702.5073386**	**724.4893**	12.85
32 :	1	40	78	8	1	1	0	731.546464	732.55374	**732.5537401**	**754.536264**	16.65
32 :	2	40	76	8	1	1	0	729.530814	730.53809	**730.5380901**	**752.520614**	14.89
34 :	1	42	82	8	1	1	0	759.577764	760.58504	**760.5850402**	**782.567564**	18.61
34 :	2	42	80	8	1	1	0	757.562114	758.56939	**758.5693902**	**780.551914**	16.95
36 :	1	44	86	8	1	1	0	787.609064	788.61634	**788.6163403**	**810.598864**	20.44
36 :	2	44	84	8	1	1	0	785.593414	786.60069	**786.6006902**	**808.583214**	18.91
IS24 :	0	32	64	8	1	1	0	621.436913	622.44419	**622.444190**	**644.426713**	9.5
IS34 :	0	42	84	8	1	1	0	761.593414	762.601239	**762.601239**	**784.583214**	20.14
IS38 :	0	46	92	8	1	1	0	817.656014	818.663839	**818.663839**	**840.645814**	23.34

Table 10: TAG mass list

Side chain			dbs	C	H	O	P	N	D	M	[M+H]+	**[M+NH4]$^+$**	**[M+Na]$^+$**	tR (min)
	42	:	0	45	86	6	0	0	0	722.642413	723.65	**740.6762342**	**745.631634**	27.96
	42	:	1	45	84	6	0	0	0	720.626763	721.63	**738.6605842**	**743.615984**	27.00
	42	:	2	45	82	6	0	0	0	718.611113	719.62	**736.6449342**	**741.600334**	25.83
	44	:	0	47	90	6	0	0	0	750.673713	751.68	**768.7075343**	**773.662934**	29.03
	44	:	1	47	88	6	0	0	0	748.658063	749.67	**766.6918843**	**771.647284**	28.13
	44	:	2	47	86	6	0	0	0	746.642413	747.65	**764.6762342**	**769.631634**	27.06
IS45		:	0	48	92	6	0	0	0	764.689363	765.7	**782.7231843**	**787.678584**	29.49
	46	:	0	49	94	6	0	0	0	778.705013	779.71	**796.7388344**	**801.694234**	30.02
	46	:	1	49	92	6	0	0	0	776.689363	777.7	**794.7231843**	**799.678584**	29.12
	46	:	2	49	90	6	0	0	0	774.673713	775.68	**792.7075343**	**797.662934**	28.20
	46	:	3	49	88	6	0	0	0	772.658063	773.67	**790.6918843**	**795.647284**	27.23
	48	:	0	51	98	6	0	0	0	806.736313	807.74	**824.7701344**	**829.725534**	30.95
	48	:	1	51	96	6	0	0	0	804.720663	805.73	**822.7544844**	**827.709884**	30.09
	48	:	2	51	94	6	0	0	0	802.705013	803.71	**820.7388344**	**825.694234**	29.26
	48	:	3	51	92	6	0	0	0	800.689363	801.7	**818.7231843**	**823.678584**	28.36
	50	:	0	53	102	6	0	0	0	834.767613	835.77	**852.8014345**	**857.756835**	31.85
	50	:	1	53	100	6	0	0	0	832.751963	833.76	**850.7857845**	**855.741185**	31.02
	50	:	2	53	98	6	0	0	0	830.736313	831.74	**848.7701344**	**853.725534**	30.26
	50	:	3	53	96	6	0	0	0	828.720663	829.73	**846.7544844**	**851.709884**	29.42
IS51		:	0	54	104	6	0	0	0	848.783263	849.79	**866.8170845**	**871.772485**	32.15
	52	:	0	55	106	6	0	0	0	862.798913	863.81	**880.8327346**	**885.788135**	32.62
	52	:	1	55	104	6	0	0	0	860.783263	861.79	**878.8170845**	**883.772485**	31.85
	52	:	2	55	102	6	0	0	0	858.767613	859.77	**876.8014345**	**881.756835**	31.16
	52	:	3	55	100	6	0	0	0	856.751963	857.76	**874.7857845**	**879.741185**	30.33
	54	:	0	57	110	6	0	0	0	890.830213	891.84	**908.8640346**	**913.819435**	33.22
	54	:	1	57	108	6	0	0	0	888.814563	889.82	**906.8483846**	**911.803785**	32.62
	54	:	2	57	106	6	0	0	0	886.798913	887.81	**904.8327346**	**909.788135**	31.92
	54	:	3	57	104	6	0	0	0	884.783263	885.79	**902.8170845**	**907.772485**	31.25
	56	:	0	59	114	6	0	0	0	918.861513	919.87	**936.8953347**	**941.850735**	33.68
	56	:	1	59	112	6	0	0	0	916.845863	917.85	**934.8796847**	**939.835085**	33.22
	56	:	2	59	110	6	0	0	0	914.830213	915.84	**932.8640346**	**937.819435**	32.69
	56	**:**	3	59	108	6	0	0	0	912.814563	913.82	**930.8489332**	**935.804363**	
IS57		:	0	60	116	6	0	0	0	932.877163	933.88	**950.9109847**	**955.866385**	33.92
	58	:	0	61	118	6	0	0	0	946.892813	947.9	**964.9266348**	**969.882035**	34.05
	58	:	1	61	116	6	0	0	0	944.877163	945.88	**962.9109847**	**967.866385**	33.68
	58	:	2	61	114	6	0	0	0	942.861513	943.87	**960.8953347**	**965.850735**	33.29
	60	:	0	63	122	6	0	0	0	974.924114	975.93	**992.9579348**	**997.913335**	
	60	:	1	63	120	6	0	0	0	972.908463	973.92	**990.9422848**	**995.897685**	34.05
	60	:	2	63	118	6	0	0	0	970.892813	971.9	**988.9266348**	**993.882035**	33.75
	62	:	1	65	124	6	0	0	0	1000.939764	1001.9	**1018.973585**	**1023.928985**	34.35
	62	:	2	65	122	6	0	0	0	998.924114	999.93	**1016.957935**	**1021.913335**	34.05
	64	:	1	67	128	6	0	0	0	1028.971064	1030	**1047.004885**	**1051.960285**	34.68
	64	:	2	67	126	6	0	0	0	1026.955414	1028	**1044.989235**	**1049.944635**	34.35
	66	**:**	1	69	132	6	0	0	0	1057.00	1058	**1075.036734**	**1079.992164**	34.88
	68	**:**	1	71	136	6	0	0	0	1085.03	1086	**1103.068034**	**1108.023464**	35.12
	70	**:**	1	73	140	6	0	0	0	1113.06	1114	**1131.099334**	**1136.054764**	35.28

Table 11: DAG mass list

Side chain	dbs	C	H	O	P	N	D	M	[M+H]$^+$	**[M+Na]$^+$**	**[M+NH4]$^+$**	tR (min)
28 :	1	31	58	5	0	0	0	510.42840	511.43623	**533.4182022**	**493.4256669**	15.88
30 :	0	33	64	5	0	0	0	540.47535	541.48318	**563.4651523**	**523.4726170**	16.68
30 :	1	33	62	5	0	0	0	538.45970	539.46753	**561.4495023**	**521.4569670**	18.08
30 :	2	33	60	5	0	0	0	536.44405	537.45188	**559.4338522**	**519.4413170**	16.35
32 :	1	35	66	5	0	0	0	566.49100	567.49883	**589.4802237**	**549.4882671**	20.07
32 :	2	35	64	5	0	0	0	564.47535	565.48318	**587.4645737**	**547.4726170**	18.38
34 :	1	37	70	5	0	0	0	594.52230	595.53013	**617.5115238**	**577.5195671**	21.81
34 :	2	37	68	5	0	0	0	592.50665	593.51448	**615.4958737**	**575.5039171**	20.31
36 :	1	39	74	5	0	0	0	622.55360	623.56143	**645.5428238**	**605.5508672**	23.5
36 :	2	39	72	5	0	0	0	620.53795	621.54578	**643.5271738**	**603.5352172**	22.04
IS36 :	0	39	74	6	0	0	0	638.5485	639.5558	**661.5377341**	**656.5828826**	23.8
IS28 :	0	31	60	5	0	0	0	512.4441	513.4519	**535.4332736**	**495.4413170**	17.71

Table 12: PI mass list

Side chain		dbs	C	H	O	P	N	D	M	[M+H]$^+$	[M-H]-	tR (min)
28	:	0	33	66	8	1	1	0	635.4525635	636.4603885	**634.4447385**	14.35
28	:	1	33	64	8	1	1	0	633.4369135	634.4447385	**632.4290885**	12.69
30	:	0	35	70	8	1	1	0	663.4838636	664.4916886	**662.4760386**	16.48
30	:	1	35	68	8	1	1	0	661.4682136	662.4760386	**660.4603885**	14.81
30	:	2	35	66	8	1	1	0	659.4525635	660.4603885	**658.4447385**	13.15
32	:	1	37	72	8	1	1	0	689.4995136	690.5073386	**688.4916886**	16.88
32	:	2	37	70	8	1	1	0	687.4838636	688.4916886	**686.4760386**	15.18
34	:	1	39	76	8	1	1	0	717.5308137	718.5386387	**716.5229887**	18.84
34	:	2	39	74	8	1	1	0	715.5151637	716.5229887	**714.5073386**	17.24
36	:	1	41	80	8	1	1	0	745.5621138	746.5699388	**744.5542887**	20.6
36	:	2	41	78	8	1	1	0	743.5464637	744.5542887	**742.5386387**	19.14
IS24	:	0	29	58	8	1	1	0	579.3899634	580.3977884	**578.3821384**	9.86
IS34	:	0	39	78	8	1	1	0	719.5464637	720.5542887	**718.5386387**	20.37